PCM energy storage during defective thermal cycling

Design of the "Capacity Cube" and modelling of PCM pouches to trace the impact of incomplete thermal cycling

S.F. Koekenbier
Final assignment, September 2011
PE 2476

Delft University of Technology
Faculty of Mechanical, Maritime and Materials Engineering
Sustainable Processes and Energy Technologies
Specialisation Engineering Thermodynamics

PCM energy storage during defective thermal cycling

Design of the "Capacity Cube" and modelling of PCM pouches to trace the impact of incomplete thermal cycling

A thesis submitted to the MSc-ME track of Sustainable Processes and Energy Technologies at the Faculty of Mechanical, Maritime and Materials Engineering in partial fulfillment of the requirements for the degree of Master of Science in Mechanical Engineering at Delft University of Technology

by

Sander Frank Koekenbier

on the authority of

dr. ir. C.A. Infante Ferreira

Copyright © 2011 by S.F. Koekenbier, Amsterdam, the Netherlands

Delft University of Technology
Faculty of Mechanical, Maritime and Materials Engineering
Sustainable Processes and Energy Technologies
Specialisation Engineering Thermodynamics

barely covered by moonlit gown
i gaze upon the world around
a view beyond a distant shore

where have i travelled farther
there shall never be another
for i will always love you more

Sander Koekenbier, 2011

ABSTRACT

Incomplete thermal cycling affects PCM storage capacities. Existing PCM measuring methods are presented with their drawbacks. A new device is designed to bypass these drawbacks. Both the new device and PCM pouches are modelled to perform simulations on full thermal cycles and on incomplete thermal cycles. Results are discussed and compared to similar methods. Recommendations are given to improve the pouch model.

SUMMARY

Phase Change Materials (PCMs) are materials that are able to store or release energy while they change phase at a constant or nearly constant temperature. Solid-liquid phase transitions are most suitable for practical thermal energy storage applications. Successive melting and freezing transitions are referred to as thermal cycling. When incomplete melting and freezing is involved PCM long term behaviour is uncertain. This work focuses on the latter drawback of PCM applications. The research question is: What is the impact of incomplete thermal cycling on the energy storage capacity of PCM pouches as applied in built environment?

Commonly applied existing measuring methods to obtain PCM thermodynamic properties are Differential Scanning Calorimetry (DSC), the T-history method and Scanning Transitiometry (ST). However these methods lack the possibility to measure bulk material samples amongst other drawbacks. The water bath method by Bouwman is able to test real pouches but uses water as heat transferring medium whereas PCM pouches in built environment are surrounded by air.

To bypass the disadvantages of existing measuring methods a new measuring device, the Capacity Cube, is designed and modelled. The Capacity Cube is named after its functional and geometrical design. The design procedure follows a morphological approach resulting in a cubical box which holds a PCM pouch in horizontal position. With a thermo-electric module the heat load to the inside air is controlled. An axial fan forces the heated air to flow around the pouch. Thermocouples and temperature transmitters monitor the temperature levels of pouch and inside air.

Both the Capacity Cube and PCM pouch are modelled to perform simulations. First the Capacity Cube is modelled and validated. Then the PCM pouch is modelled and validated. Finally both models are assembled to simulate full thermal cycles and half thermal cycles. Simulation outputs are enthalpy-temperature graphs. These graphs clearly show that PCM exhibits inhomogeneous behaviour. Melting and freezing curves coincide for pure, single phases only. It is this inhomogeneous behaviour that also explains the sudden enthalpy increase at the start of phase change. As phase change for the full pouch finalizes the enthalpy curve loses its steepness and flattens out towards the straight line

representing the specific heat. Defective thermal cycling does affect the storage capacity significantly. For half cycles the storage capacity halves likewise. Regarding the steepness of the enthalpy-temperature curves, it is expected half cycles correspond with more than half of the energy accumulation, however this is not supported by simulation results.

Since real time measurements are not carried out, it is recommended to build a Capacity Cube prototype to perform experiments with. Moreover the PCM pouch model should be augmented to account for aging effects and to yield improved enthalpy curves within the phase change region.

TABLE OF CONTENTS

Table of Contents [continued]

LIST OF SYMBOLS

Symbol	description	units
A	surface area	m^2
Bi	Biot number	-
c	specific heat	J/kgK
D	diameter	m
d	thickness	m
d	differential	-
E	energy	W, J
F	view factor	-
f	massflow	kg/s
g	gravitational acceleration	m/s^2
Gr	Grashof number	-
H	height	m
H	enthalpy	J
h	specific enthalpy	J/kg
L	length	m
m	mass	kg
N	number of holes in grid	-
Nu	Nusselt number	-
P	perimeter	m
p	pressure	Pa
Pr	Prandtl number	-
Q	heat transfer	W, J
R	reference material	-
Ra	Rayleigh number	-
Re	Reynolds number	-
S	sample material	-
T	temperature	K
t	time	s, h
V	volume	m^3
v	velocity	m/s
W	width	m
x	input vector	-
y	output vector	-
z	parameter vector	-

List of symbols [continued]

Greek letters	description	units
α	heat transfer coefficient	W/m^2K
β	volumetric expansion coefficient	K^{-1}
Δ	difference	-
δ	thermal diffusivity	m^2/s
δ	partial differential	-
ε	emissivity	-
φ	volume flow	m^3/s
λ	thermal conductivity	-
μ	dynamic viscosity	Pa.s
ν	kinematic viscosity	m^2/s
ρ	specific mass	kg/m^3
σ	Stefan-Boltzmann constant	W/m^2K^4
θ	temperature	°C

Subscripts

aver	average
C	convection
D	conduction
D	diameter
F	flow
f	film boundary layer
flow	air flow
free	free convection
forced	forced convection
in	in, entering
i	index
L	(characteristic) length
lat	latent
liq	liquid
m	surface m
m	melt
mixed	combined free and forced convection
m-n	from surface m to n
n	surface n
n-m	from surface n to m
out	out, leaving

List of symbols [continued]

Subscripts

p	constant pressure (isobar)
pc	phase change
PCM	phase change material
pouch	PCM pouch
R	radiation
S	surface
sol	solid
surr	surroundings
T	constant temperature (isotherm)
V	constant volume (isochoor)
wall	Capacity Cube envelope wall
1	state 1
2	state 2
∞	fully developed flow conditions
,	subscript separator

Superscripts

j	time instant
j-1	previous time instant
$\bar{}$	surface average conditions (overbar)

Abbreviations and acronyms

CC	capacity cube
CO_2	carbon dioxide
DSC	differential scanning calorimetry
DTA	differential thermal analysis
ECN	Energy Research Centre Netherlands (Dutch: Energieonderzoek Centrum Nederland)
e.g.	for example (Latin: exempli gratia)
et al.	and others (Latin: et alii)
EPS	expanded polystyrene

List of symbols [continued]

Abbreviations and acronyms

FBD	function block diagram
HVAC	heating ventilation & air conditioning
i.e.	that is (Latin: id est)
MIT	Massachusetts Institute of Technology
PCM	phase change material
PCMs	phase change materials
Pt	platinum
R	reference
RAL	German State Committee for terms of Delivery and Sale (German: Reichs-Ausschuß für Lieferbedingungen)
RH	relative humidity
S	sample
TT	temperature transmitter
vol.	volume

1 INTRODUCTION

Phase Change Materials (PCMs) are materials that are able to store or release energy while they change phase at a constant or nearly constant temperature. As such, PCMs can be used to buffer thermal energy or to moderate temperature variations. Farid et al. [19, 20] combined a PCM layer with an electrical floor heating system (figure 1.1). By applying the PCM layer they levelled out heat transfer rates to the room and maintained the floor surface temperature close to 24 [°C] for about eight hours.

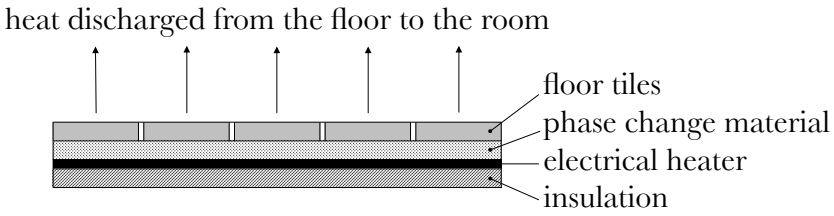

figure 1.1 *Schematic of domestic floor heating system with PCM [19, 20]. Because of the PCM layer applied in the floor heating system the floor surface temperature remains 24 [°C] for about eight hours. Without PCM the temperature increases up to 36 [°C].*

Section 1.1 further continues on theory and backgrounds of PCM and its applications. Next section 1.2 addresses the problem statement. In section 1.3 the purpose of the presented work is explained. Last section 1.4 clarifies the thesis' contents and structure.

1.1 Background

Phase transitions in general comprise chemical phase changes by breaking and restoring intermolecular connections as well as physical phase changes from solid to solid, solid to liquid, solid to gas and liquid to gas or vice versa [27, 29]. Chemical phase change offers more energy storage per unit of mass than physical phase change does, however physical processes are fully reversible. Solid to solid phase transitions usually do not meet the heats

of fusion required for practical thermal energy storage whereas phase changes involving gaseous materials require inconveniently large volumes and high pressures [10, 27]. In case of solid-liquid phase transitions the volume changes are comparatively small and the amount of thermal energy stored with solid-liquid phase transitions is relatively large over a limited temperature range [27, 29]. Therefore solid-liquid phase transitions are most suitable for practical thermal energy storage applications.

Sensible heat storage is the quantity of energy stored when one kilogram of material increases one degree in temperature. Latent heat storage is the quantity of energy stored when one kilogram of material changes phase at uniform temperature. During phase change PCMs store or release both latent and sensible heat, however latent heat exchange prevails. The efficiency of latent heat storage over sensible heat storage is clearly shown by the following example.

At atmospheric pressure 4.18 [kJ] of energy is needed to raise 1 [kg] of water from 0 [°C] to 1 [°C]. Otherwise stated; the sensible heat absorbed by water when increased a degree in temperature is 4.18 [kJ/kg] (figure 1.2, top). Comparatively 1 [kg] of ice at 0 [°C] requires 334 [kJ] to transfer into water of 0 [°C]; the latent heat absorbed by water when turning from solid to liquid is 334 [kJ/kg] (figure 1.2, bottom). So in case of water and ice the quantity of energy stored by means of latent heat is about 80 times larger than the quantity of energy stored by means of sensible heat.

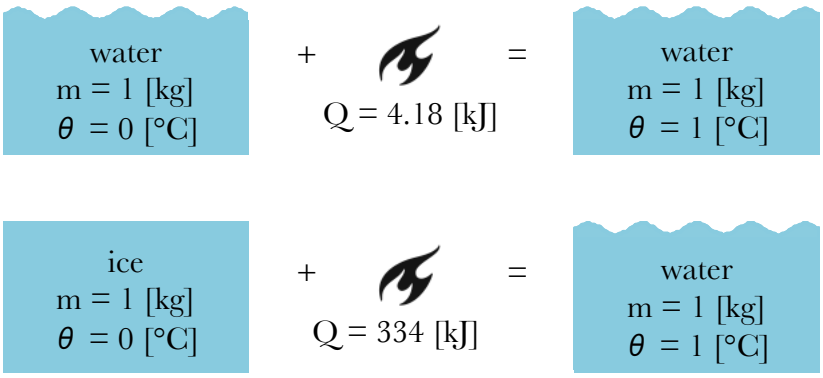

figure 1.2 *Comparison of H_2O sensible heat storage (top) and latent heat storage (bottom). As H_2O transfers from solid (ice) to liquid (water) the amount of energy stored is about 80 times higher than during a 1 degree temperature rise in the liquid phase.*

Water is an example of a PCM that changes phase at 0 [°C]. During melting, as the PCM undergoes a solid to liquid transition, energy is being stored. When the process reverses the material solidifies and energy is being released again. Phase change materials mainly utilize the enthalpy change of phase transitions to store energy [10, 42]. However, like any other material, PCMs also dispose of a sensible heat storage part. PCMs utilize sensible heat

storage above and below their phase change temperatures [29]. The total heat stored by the material during phase change is given by [61]:

$$Q_{PCM} = m\left[\int_{T_1}^{T_{pc}} c_{p,sol}(T)dT + (h_2 - h_1) + \int_{T_{pc}}^{T_2} c_{p,liq}(T)dT\right] \quad (1.1)$$

Where the first term on the right hand side is the sensible heat part for the solid state, the second term represents the latent heat of phase change, and the third term is sensible heat part for the liquid phase of the PCM. Regarding practical heat storage systems the latent heat storage predominates, but sensible heat storage can significantly contribute to the total heat stored, especially for increasing operating temperature changes.

Amounts of energy storage per unit mass depend on the PCM composition. By altering the compositions of PCMs the phase transition temperatures are customized to satisfy their applications. figure 1.3 gives an overview of different classes of PCMs and their latent heats as a function of melting temperatures.

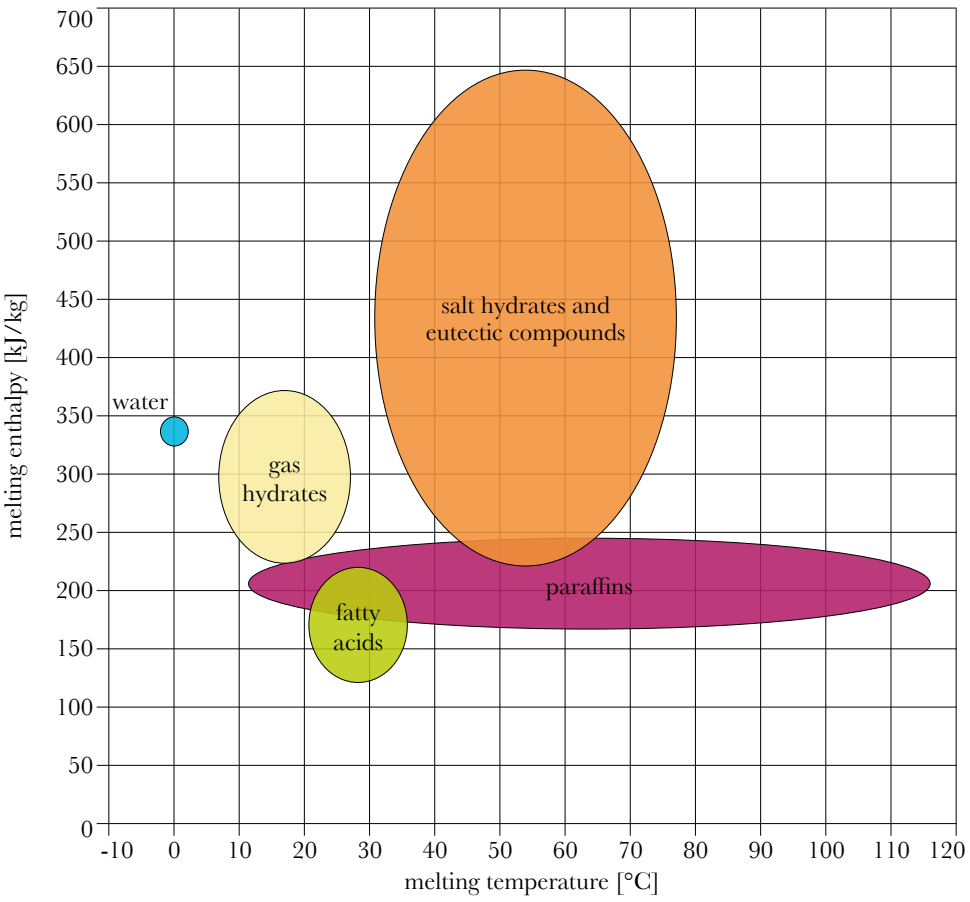

figure 1.3 *Heat of fusion versus melting point for commonly applied PCMs in the temperature range from 0 [°C] to 120 [°C], derived from Hauer et al. [28].*

Isothermal phase change is often assumed, e.g. [1, 9], but only for pure materials and some eutectics the phase change temperature is constant [70]. Also most salt hydrates expose isothermal phase transition [72]. Practical applicable phase change materials are composites, mixtures, alloys or compounds. Since these PCMs consist of two or more substances they melt and solidify within a certain temperature range.

1.2 Problem definition

Late 1940s Maria Telkes used to be a research associate at Massachusetts Institute of Technology (MIT) when she became one of the pioneers in the field of latent heat storage. Telkes finished the construction of the very first PCM heated house with befriended architect Eleanor Raymond in 1948. After three years the house failed because the utilized PCM lost most of its energy storage capacity. Although it has been sixty years since Telkes' effort failed, the problems she encountered are still of importance today when one is developing a PCM storage system.

Both passive and active PCM applications in buildings, especially PCM enhanced HVAC or cooling systems, are able to reduce CO_2 emissions and save energy [38, 48] however simulations on PCM enforced buildings as a whole have not been carried out frequently [32]. Problems with PCM applications often arise when improper phase change materials are selected or when inappropriate PCM incorporated materials are used [39, 61]. Such deficiencies can lead to incomplete melting or solidification so that heat or cold is stored insufficiently. Free cooling can result in incomplete melting or solidification as well so that the actual performance of the selected PCM differs from the theoretical performance as predicted by the manufacturer [2]. Moreover knowledge of PCM phase change behaviour on a macroscopic scale is essential for selecting the right material and developing sustainable energy storage systems [9].

Successive melting and freezing transitions are referred to as thermal cycling. In the long run thermal cycling affects the heat storage capacity of PCMs significantly [57, 59, 72]. Thermal cycling is often mentioned in papers [e.g. 24, 57] as part of modelling efforts and measurements or as a recommended future research item but few long term thermal cycling projects have been reported in literature. Exceptions are for example Bach and Haije [3] and Shukla et al. [59]. Since thermal cycling tests require live daytime simulations some researchers conduct accelerated tests or perform relatively short tests ranging from several days up to a few years [37, 58, 65]. However, as encountered by Telkes' Dover House, problems still can arise after three years or more.

To summarize, PCMs that are applied in HVAC systems or building envelopes reduce CO_2 emissions while they decrease the need for conventional energy resources. However, long term behaviour is uncertain, especially when incomplete melting and freezing is involved. This work focuses on the latter alleged drawback of PCM applications. The research question is: What is the impact of incomplete thermal cycling on the energy storage capacity of PCM pouches as applied in built environment?

1.3 Objectives

First objective is to design a test facility for live size PCM pouch measurements. The device should be able to reverse or interrupt pouch thermal cycle to determine the influence on the PCM energy storage. Second goal is to model both the test facility and PCM pouch to conduct simulations that gain results, which support to answering the research question. Besides existing measuring methods are described to give an overview an provide the reader with an insight into aspects that have to be taken into account when developing a new test facility.

1.4 Outline

Subject of chapter 2 are the existing measurement techniques to obtain thermodynamic properties of materials, specifically PCMs. Chapter 3 continues on the design of the Capacity Cube, as the new test facility is called, referring to its functional and geometrical design. The Capacity Cube model is addressed in chapter 4, followed by the modelling approach for the PCM pouch in chapter 5. Simulation results are discussed in chapter 6. Final chapter 7 presents conclusions and gives recommendations for future work.

2 MEASURING METHODS

Thermophysical properties like latent heat, specific heat, density and conductivity, are often utilized to mutually compare PCMs. However accurate PCM measurements are not possible with standards developed for materials that do not experience phase transitions. Consequently Mehling et al. [46] described suitable measuring methods and compiled a standard on PCM data presentation from which a PCM quality label has been extracted that is in use by the RAL Gutegemeinschaft [50]. Appropriate measuring methods to obtain the PCM thermophysical characteristics mainly comprise differential scanning calorimetry (2.1) and the T-history method (2.2) [26, 30]. Scanning transitiometry (2.3) shows similarities to DSC and the T-history method, but it offers more possibilities to adjust output variables. Finally the water bath method (2.4) bypasses several drawbacks of DSC, T-history and transitiometry techniques. A discussion on drawbacks of existing methods closes this section (2.5).

2.1 Differential scanning calorimetry

Differential Scanning Calorimetry (DSC) is a thermoanalytical measuring technique which determines differences in heat transfer rates between a sample product and a reference product. These differences are caused by either physical or chemical transformations that the sample undergoes like phase transitions. As such the measured differences in heat transfer give useful information about the physical state and thermal behaviour of the sample as well as data on thermodynamic properties like heat capacity and enthalpy are provided. This section is based largely on the book by Dodd and Tonge [11] and on the DSC description by the Energy Research Centre of the Netherlands (ECN) [18]. Other resources are indicated individually.

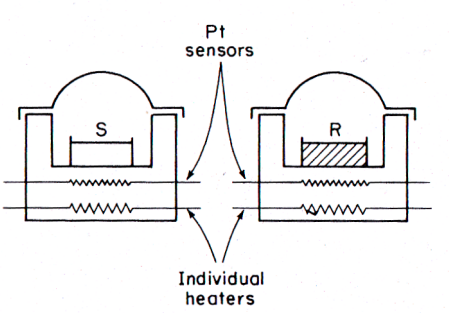

figure 2.1 *Schematic of differential scanning calorimeter [11]. During heating the temperatures of both the sample (S) and reference (R) materials are measured to acquire information on the thermodynamic properties of the sample piece.*

The measuring device – a differential scanning calorimeter (figure 2.1) – is a thermally insulated box which heats up its contents as it controls the inside temperature. The differential scanning calorimeter operates in the temperature range from -150 [°C] to 700 [°C]. In practice the differential scanning calorimeter measures the temperature difference between sample and reference. To attain information on the heat flows corresponding to the temperature fluctuations the differential scanning calorimeter uses an operation analogue to Ohm's Law. The calorimeter contains two pieces of material; a sample piece which is under investigation, and an inert reference piece of which the heat capacity over the temperature range to be measured is known. As the calorimeter maintains both pieces at the same temperature, less or more heat will transfer to the sample when it undergoes a phase transition. Now three situations can occur with respect to the sample:

- no reaction or transition takes place
- an endothermic reaction or transition takes place
- an exothermic reaction or transition takes place

When the sample undergoes no reaction or phase transition the net temperature difference between reference and sample equals zero. The calorimeter measures no heat flow at all.

As the sample undergoes an endothermic reaction or phase transition, like melting from solid to liquid, it requires more heat to increase the sample temperature at the same rate as the temperature of the reference piece increases. The calorimeter measures heat transfer towards the sample.

When the sample undergoes an exothermic reaction or phase transition, like crystallization from liquid to solid, it requires less energy to decrease the sample temperature at the same rate as the temperature of the reference piece decreases. The calorimeter measures heat transfer from the sample.

The DSC curve shown in figure 2.2 is idealised to show three processes which are clearly observable in DSC. On the ordinate the heat input to the sample is expressed against the temperature on the abscissa. The area under a melting endotherm is proportional to the latent heat of fusion of the sample. Crystallization processes yield exothermic peaks and melting processes are visible by endothermic peaks. A step in the baseline is not caused by a formal phase change but due to a change in heat capacity the sample exhibits.

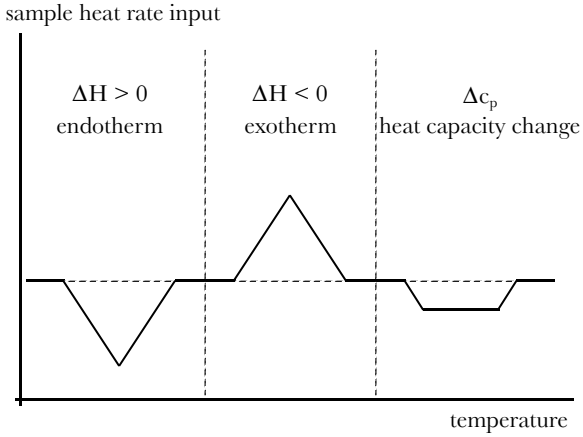

figure 2.2 Idealized DSC curve (reproduced from Dodd and Tonge [11]).

A corresponding technique to DSC is differential thermal analysis (DTA). DTA and DSC yield similar results and give the same kind of information. DSC more often involves quantitative measurement in terms of energy changes. DTA allows a temperature difference to develop between the reference and sample material. DSC measures the heat flow required to keep the temperatures the same.

Data on PCMs heat storage capabilities can also be attained by DSC via isothermal step measurement [26]. In this case the sample material responses with some delay to a stepwise heat input by the furnace (figure 2.3). Because of the delayed response a signal can be detected. As soon as the signal is levelled out the sample and furnace are in thermal equilibrium. Then the next step takes place until thermal equilibrium is reached again. Addition of the step values yields the heat storage capacity or, by differentiation, the enthalpy curve h(T) of the sample PCM.

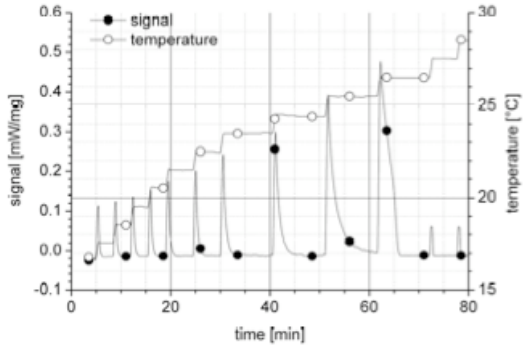

figure 2.3 DSC isothermal step curve [adapted from 26].

Although DSC is well developed, it is not possible to measure samples simultaneously, and during measurements actual phase change processes of sample materials are hard to observe. The major shortcomings are [13, 26, 71]:

- samples are relatively small; up to 25 [mg]
- manifestations of sub- and supercooling effects cannot be detected
- only homogeneous samples can be used

All three deficiencies affect PCMs, because practical PCM applications involve bulk materials that have thermophysical properties different from such small samples. Moreover many PCMs, salt hydrates in particular, manifest some degree of supercooling. And last, since phase transitions involve coexistence of multiple phases, PCMs are not homogeneous in their critical working range.

2.2 T-history method

In view of the disadvantages of conventional calorimetry methods, DSC and DTA in particular, Zhang and others developed an improved PCM measuring method; the T-history method. The method is named after the temperature time curve, the T-history curve that is which comes as a result of the measurements carried out with this method. With the T-history method it is possible to determine specific heat, melting point, thermal conductivity, and heat of fusion of PCM. Features of the t-history method are [71]:

- several PCM samples may be measured simultaneously
- actual phase change process is observable
- simple unit set up

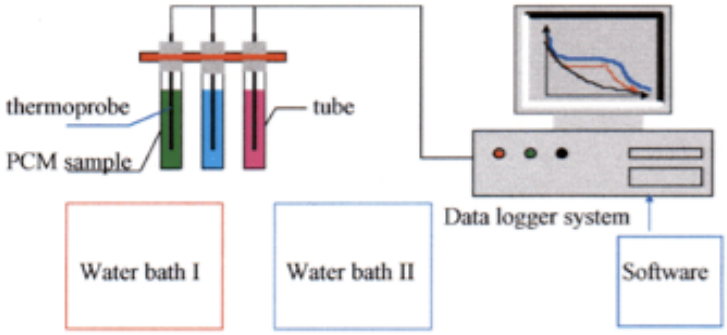

figure 2.4 Schematic of T-history test setup [71].

A schematic overview of the T-history test facility is shown in figure 2.4. Several PCM samples and one reference sample are investigated. Usually the reference sample contains water, but any kind of material is possible as long as its thermophysical properties are known. All samples are geometrically identical. Zhang et al. use cylindrical glass tubes that are 180.6 [mm] long and have a diameter of 10.4 [mm]. For the measurements on specific heats and heats of fusion the cooling medium is conditioned room air and water is used as reference sample. For the measurements regarding thermal conductivities the cooling medium is cold water whereas mercury is used as reference sample because of its high thermal conductivity.

During the tests molten PCM samples together with reference samples are put in a controlled environment, i.e. cool water or conditioned air with a temperature lower than the melting temperature of the PCM samples. Then both the sample and reference tubes passively exchange heat with the environment while their temperatures are being measured. From the T-history curves the thermophysical properties of the PCM samples can be calculated when these curves are compared to the T-history curves of the known reference materials. Typical T-history cooling curves obtained with this method are shown in figure 2.5, without and with supercooling respectively.

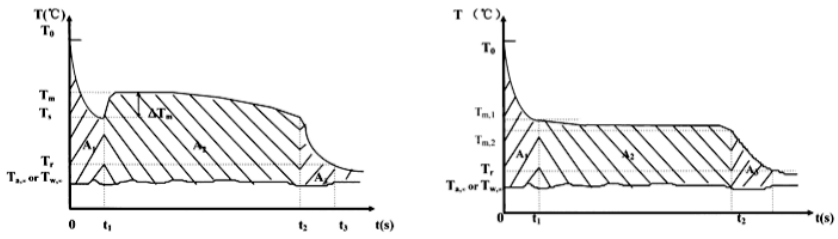

figure 2.5 T-history curve with supercooling (left) and without supercooling (right) [71].

Although the T-history method has some advantages over conventional calorimetric methods like the use of larger samples, lower cooling rates of the samples, and free heat exchange between samples and environment [13], there are two major drawbacks:

- specific heats and heats of fusion are assumed to be temperature independent variables [44]
- sensible heat is neglected during phase change [30]

Consequently the T-history method proposed by Zhang et al. is particularly appropriate for pure materials and materials with a clearly marked phase change region. However most PCMs of interest are impure and their solid and liquid state limits are not clearly expressed. Marin et al. [44] as well as Hong et al. [30] modified the T-history method to overcome these deficiencies.

Marin et al. [44] altered the energy balances of Zhang et al. [71] to use enthalpy temperature relations instead of temperature time variations. By varying the temperature over small intervals and determining the enthalpy slope at that specific temperature interval Marin et al. were able to calculate the PCM's specific heat at every point. So specific heat values as a function of temperature were obtained [44].

Zhang et al. [71] pointed the end of PCM's phase change by adopting the level of supercooling. But the supercooling degree does not depend on the end of phase change, instead it varies with cooling rate and purity of the PCM, for instance. Hence Hong et al. [30] use the minimum of the T-history curve first derivative as phase change boundary. This is reasonable since the temperature decreases only slightly during latent heat transfer, but decreases exponentially in sensible heat associated cooling processes [30].

2.3 Scanning transitiometry

The scanning transitiometry method takes its name from scanning the changes of thermodynamic functions in relation to physical or chemical transitions of a certain substance [52]. Although scanning transitiometry resembles calorimetry methods, it stands out in the determination of both mechanical and thermal responses to variations of an independent thermodynamic variable of state (p, V or T), as the other state variable remains constant. The thermal and mechanical equations of state for the investigated material are directly derived from the relation between the scanned independent variable and the dependent variable, as shown in figure 2.6 [36].

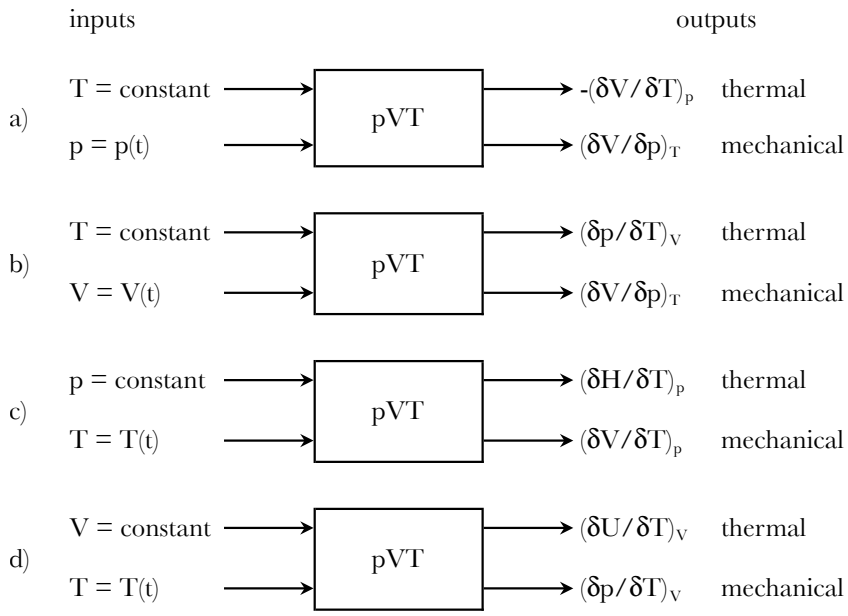

figure 2.6 *Diagram representing the input and output variables to four scanning transitiometry measurements (reproduced from [36]).*

As heat flow and volume changes are scanned, four situations are distinguished [52]:

a) pressure varies at constant temperature yielding the isobaric thermal expansivity and the isothermal compressibility
b) volume varies at constant temperature giving the temperature coefficient of pressure and the isothermal compressibility
c) temperature varies at constant pressure giving the isobaric heat capacity and the isobaric thermal expansivity
d) temperature varies at constant volume giving the isochoric heat capacity and the temperature coefficient of pressure

Relatively wide temperature and pressure ranges characterize the scanning transitiometry method. The operating temperature reaches from 173 [K] to 673 [K] whereas the operating pressure reaches from 0.1 [MPa] up to 400 [Mpa] [25]. The sample volume varies from 0.5 [cm^3] to 2.5 [cm^3] [51] as the typical sample mass ranges up to about four grammes [47]. In scanning transitiometry measurements a sample vessel is compared to a reference vessel. Both vessels are tubes of 0.8 [cm] internal diameter for measurements up to 200 [Mpa], and 0.48 [cm] internal diameter tubes for measurements up to 400 [Mpa] [25, 51]. The sample vessel is connected to the pressure / volume regulator while the reference vessel acts as a thermal reference only. A calorimeter encloses both the sample and reference vessels so that thermocouples are able to directly control the temperature. A stepping motor drives the pump which controls the pressure and volume variations. Characteristic property changes are [36]:

- temperature: 0.1 [mK/s] – 5 [mK/s]
- volume: $5 \cdot 10^{-6}$ [cm³/s] – $5 \cdot 10^{-3}$ [cm³/s]
- pressure: 0.001 [Mpa/s] – 0.05 [Mpa/s]

Scanning transitiometry is specifically useful for studying phase transitions when significant pressure changes are involved. [52]. However the method shares the drawback of relatively small sample sizes with conventional calorimetry methods and the T-history method. Moreover the scanning transitiometry applies to homogeneous samples only to obtain the thermomechanical coefficients [25].

2.4 Water bath method

Rydstrand et al. [56] constructed an experimental setup to test phase change materials in a variety of geometries and over different temperature intervals. The tested PCM capsules are immersed in a 0.3 [m³] storage tank which is filled with water. The temperature inside the tank can be controlled between 0 [°C] and 40 [°C] by means of a chiller, a heater and a pump which regulates the water flowrate up to 0.5 [dm³/s]. Flow rates and water temperatures are measured and analysed but during a first experiment on 120 PCM pouches of 0.5 kg each it became clear that these temperature and flow data could not provide sufficient information on the actual phase transition. Therefore a smaller experiment was carried out. In this smaller experiment two plate-shape, tightly connected pouches of PCM are placed in a $50 \cdot 10^{-3}$ [m³] water tank. At first the water is cooled from ambient temperature to 0 [°C], then the water temperature is kept constant and at last, under influence of heat transfer from the environment, the water temperature rises again. A sensor measures the PCM temperature in between the two pouches. figure 2.7 depicts Rydstrands results regarding a test with Climsel 7 PCM which is commercially available.

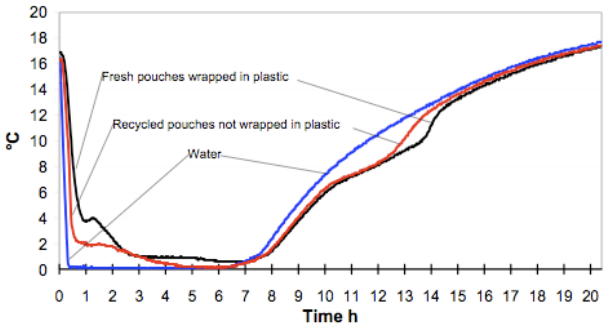

figure 2.7 Temperature measurements of PCM pouches and water [56].

With the setup and method as proposed by Rydstrand et al. [56] the phase change temperature as well as the phase change temperature range are hard to predict [56]. Moreover, the output consists of a temperature-time graph only, whereas PCM are most often compared by their heat capacities and latent heat storage capabilities.

Bouwman developed a new method to test PCM pouches and to obtain $c_p(T)$ and $h(T)$ graphs from PCM measurements [6]. Bouwman's 'water bath method' is based on the experimental setup used by Rydstrand et al. In advance to developing the water bath method Bouwman considered the following aspects which generally apply to PCM test facilities:

- measuring the core temperature of PCM pouches is complicated since pouches cannot be opened or pierced because the PCM composition may change when exposed to water or air
- temperature distribution in the PCM should be prevented to ensure that the measured temperature represents the temperature of the total pouch
- the energy transfer rate between a typical PCM pouch and its environment is in the order of 1 – 2 [W]. When testing a single PCM capsule the measurement setup should be constructed in such a way that latent and sensible effects can be separated from the applied heat transfer
- the heat capacity of large heating equipment is higher than the heat capacity of small equipment, therefore larger equipment causes more disturbance to heat capacity measurements than small equipment. However, in case of compiled PCM pouches, larger equipment is needed to increase flow rates so that temperature distributions do not occur over the PCM stack. So these two aspects should be balanced.

With the water bath method static and dynamic behaviour of PCM are tested separately. Consequently this method comprises two parts: the static part focuses on the passive heat exchange between water and PCM (figure 2.8, left); the dynamic part focuses on the forced heat exchange between water and PCM (figure 2.8, right).

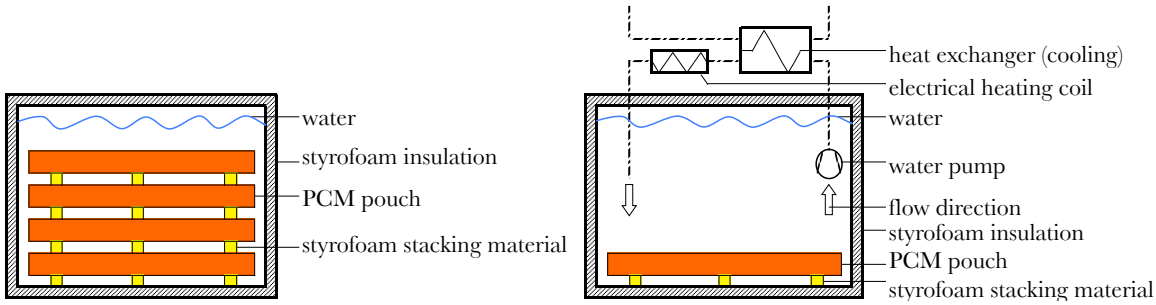

figure 2.8 *water bath schematic setup static part (left); dynamic part (right) (reproduced from Bouwman [6]).*

In the static part the heat capacities are determined. Therefore hot water and cold PCM pouches are put together in an insulated casing (figure 2.8, left). Initially PCM is in solid state and the water temperature is around the maximum allowable PCM temperature. Then heat is passively transferred from the water to the PCM pouches until equilibrium is reached. The amounts of water and PCM are chosen such that the equilibrium temperature is higher than the PCM phase change temperature.

The heat capacity of the PCM is determined from the calculated heat exchange and from temperature measurements. A larger waterside temperature difference, that is a higher water temperature change, gives the most accurate results for the heat capacity values.

In the dynamic part the heat transfer is determined. Again water and PCM are put into an insulated casing (figure 2.8, right), but here a forced water flow, that can be cooled or heated, dynamically transfers heat with the PCM pouch. Initially PCM is in solid state and water and PCM temperatures are equal, though lower than the initial PCM temperature of the static test. Then water is heated to a temperature higher than the equilibrium temperature of the static test. Because the circulation rate of water is high and the mass proportion of PCM versus water is low, water properties can be treated as lumped parameters and temperature distributions over the PCM pouch are omitted.

PCM and water temperatures are measured during this dynamic test, resulting in a temperature-time graph which is similar to the one obtained by Rydstrand. However, Rydstrand did not derive enthalpy temperature and specific heat temperature relations from his findings.

Since heat transfer by convection is ruling and temperature differences between water and PCM are relatively small, Bouwman assumes a linear relationship between the temperature difference and the overall heat transfer rate. Integration of the temperature difference over the range as applied at the static test yields a scaling factor by which the amount of transferred heat can be calculated at every time interval. As such, the combination of both tests results in the characteristic enthalpy temperature and specific heat temperature diagrams of the tested PCM.

Bouwman reports the following advantages of the water bath method:

- many different cooling and heating rates are possible
- the method is relatively cheap and fast
- samples are realistic in size
- hysteresis and sub-cooling phenomena can be observed

2.5 Discussion

Existing research devices or commercially available measuring methods carry out experiments on PCM samples that are much smaller in size and mass than the PCM units applied in practice. Small PCM samples expose thermophysical behaviour deviating from PCM bulk material. Hence there is a need for a test facility that carries out measurements on live size PCM pouches, like the devices Rydstrand [56] and Bouwman [6] developed. However both facilities use water as surrounding medium whereas PCMs in built environment are usually subjected to air flows instead of water flows. Consequently there is a need for a test facility that investigates PCM pouches which exchange heat with surrounding air.

3 CAPACITY CUBE DESIGN

The Capacity Cube (CC) is a newly designed measuring device which puts live size PCM pouches to the test by using air as heat transferring medium. This chapter addresses the design procedure for the Capacity Cube. The procedure follows a design method described by Van den Kroonenberg and Siers [40] which is based on Zwicky's morphological analysis [74]. Three phases characterize the design method:

1) functional design (problem definition phase)
2) operational design (operation determinative phase)
3) constructional design (design phase)

At first, the functional design phase (3.1) gives the motive and objective for designing the Capacity Cube. Then a schedule of requirements is compiled which states the conditions that apply to the Capacity Cube. The schedule of requirements results in a function block diagram representing all functions the Capacity Cube needs to fulfill.

The operational design phase (3.2) departs from the function block diagram. Every function can be executed by a number of operations, some for better, some for worse. The operational design phase aims for the best ways to perform the functions as well as it intends to find the appropriate combination of operations to carry out the Capacity Cube functions to the full extent.

In the constructional design phase (3.3) the combination of appropriate operations by function is further developed. Geometry and material aspects are attuned to come to the final equipment lay out. The constructional design phase is concluded by the final Capacity Cube design.

3.1 Functional design

Purpose for designing the Capacity Cube is to support the modelling process that comprises both the PCM pouch model and the Capacity Cube model. After finalizing the design a detailed model of the Capacity Cube will be set up. Moreover the design will provide a blueprint for building the Capacity Cube. In general the Capacity Cube carries out heat capacity and temperature measurements on live size PCM pouches to trace the impact of incomplete thermal cycling on the energy storage capacity of PCM pouches as applied in built environment.

The Capacity Cube should meet a number of requirements which are defined by fixed conditions, variable conditions and desirable conditions. Fixed conditions are described in terms of quantitative properties that apply strictly. Variable conditions are described in terms of upper- or lower limits and apply to more or lesser extent. Desirable conditions are described in terms of qualitative properties that are not strictly necessary but do affect the final design. All conditions are gathered in the schedule of requirements (table 3.1).

table 3.1 *Schedule of requirements. If applicable, all conditions are in accordance with indoor climate conditions, within human comfort ranges. CC stands for Capacity Cube.*

	requirement	condition
1	the CC is for indoor use only	fixed
2	the CC measures PCM pouches applicable to indoor built environment	fixed
3	the CC uses air as the medium that surrounds the PCM pouches	fixed
4	the CC contains live size PCM pouches	fixed
	a) pouch length: 80 [mm] ≤ L ≤ 1000 [mm]	variable
	b) pouch width: 80 [mm] ≤ W ≤ 450 [mm]	variable
	c) pouch thickness: 10 [mm] ≤ d ≤ 25 [mm]	variable
5	the CC is of cuboidal shape	desirable
6	the CC applies heating and cooling loads at built environment conditions	fixed
	a) heat transfer to the pouch: 50 [W/m^2] ≤ Q ≤ 200 [W/m^2]	variable
	b) heat transfer from the pouch: 20 [W/m^2] ≤ Q ≤ 120 [W/m^2]	variable
7	the CC controls the surrounding air within human comfort conditions	fixed
	a) air temperature: 18 [°C] ≤ θ ≤ 28 [°C] (during working hours)	variable
	b) air relative humidity: 30% ≤ RH ≤ 70% (during working hours)	variable
8	the CC measures PCM pouch specific heat in purely solid and purely liquid	fixed
	a) overall air temperature range: 5 [°C] ≤ θ ≤ 50 [°C]	variable
	b) overall air relative humidity range: 10% ≤ RH ≤ 90%	variable
9	the CC applies air speeds that cause no draft as experienced by humans	fixed
	a) air speed: 0.15 [m/s] ≤ v ≤ 0.25 [m/s]	variable
10	the CC uses commercially available electrical current input	fixed

Each requirement in the schedule of requirements points to a partial objective of the Capacity Cube. In order to achieve these objectives the Capacity Cube executes functions that correspond with the particular requirements. The function block diagram (figure 3.1) decomposes the prime and main functions into subfunctions, resulting in a functional description of the Capacity Cube.

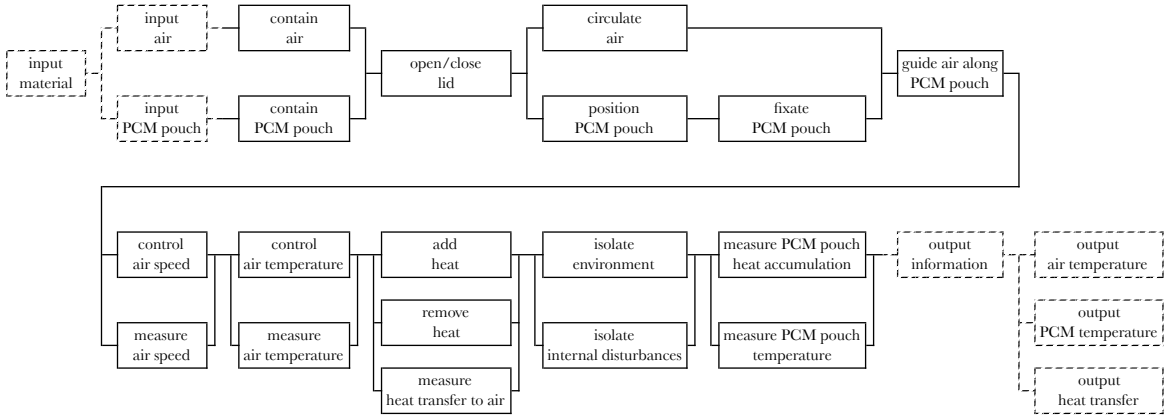

figure 3.1 *Function block diagram (FBD) representing the functions of the Capacity Cube in logical order. The FBD can be read as a flow chart. Top left starts with the material input, bottom right ends up with the output signals – both depicted within dashed contoured blocks. Functions like "isolate environment" apply throughout the whole process, however they are shown where they are most effective.*

Note that the function block diagram depicts the input and output functions within dashed contour blocks. These functions surpass the Capacity Cube system boundaries. Moreover the function block diagram only represents the functions directly related to the Capacity Cube operations. In practice the Capacity Cube requires additional functions, for example to calibrate the system, but such indirect functions are omitted here.

3.2 Operational design

Every function in the function block diagram can be accomplished by different solutions, that are operations based on physical phenomena. Though some solutions suit the particular function better than other solutions do. Also one operation that fits a certain function may counteract with operations that fit other functions. The operational design phase aims for selecting those solutions that suit best the functions from the function block diagram. Furthermore the ultimate objective here is to find an appropriate combination of operations to carry out the whole of the Capacity Cube functions. It is this combination of solutions that determines the final design structure.

To analyze the different functions and corresponding solutions a morphological chart is being used. Morphological analysis as introduced by Zwicky [74] is "nothing more than an orderly way of looking at things" [73]. The design method does not imply that all possible solutions are considered. However the solutions chosen by morphological analysis are rational and fundamental.

The morphological chart (figure 3.2) presents the Capacity Cube functions from top to bottom. Possible operations by function are shown from left to right. Initially the solutions are arbitrarily given an order of preference ranging from one to five, where one is the most preferred solution and number five stands for the least preferred solution in relation to the regarding function. Preferences are judged by simplicity, minimization of components and functionality. Solutions of first and second order preferences interconnect to create combinations of operations that satisfy the function block diagram. Three operational combinations arise (figure 3.3):

- the "purple" combination, referring to the purple line in figure 3.3 which interconnects all solutions of first order preference
- the "orange" combination, referring to the orange line in figure 3.3 which interconnects all solutions of second order preference
- the "blue" combination, referring to the blue line in figure 3.3 which interconnects a combination of solutions of both first and second order preference

function	solution				
contain air					
	open cubic box (3)	closed cubic box (1)	closed cylindrical box (2)	open cylindrical box (4)	bag (5)
contain PCM pouch					
	open cubic box (3)	closed cubic box (1)	closed cylindrical box (2)	open cylindrical box (4)	bag (5)
open / close lid					
	tighten by geometry (1)	lay upon by gravity (4)	hinge junction (3)	bolt (2)	tie (5)
circulate air					
	fan (2)	buoyancy (1)	compression (3)	suction (4)	
position PCM pouch					
	horizontal (1)	vertical (2)	diagonal (3)		
fixate PCM pouch					
	lay down (1)	pole support (4)	hang (2)	groove support (3)	frame support (5)
guide air along PCM pouch					
	pressure chamber (3)	grid (1)	duct (4)	slots (2)	
control air speed					
	volume flow valve (3)	pressure valve (4)	frequency controlled fan (2)	adjust geometry (1)	
measure air speed					
	anemo mill (2)	pressure difference (3)	cooling thermocouple (4)	derive from air speed control (1)	
measure air temperature					
	sensors (2)	analogue thermometer (4)	reference material (3)	thermocouples (1)	
add heat					
	sun radiance (5)	indirect water heating (3)	thermo electrical heating (1)	direct gas heating (4)	heat from components (2)
distract heat					
	direct water cooling (4)	ice cooling (5)	indirect water cooling (2)	refrigerant cooling (3)	thermo electrical cooling (1)
determine heat transfer to air					
	derive from energy input (3)	derive from air temperature (1)	derive from heat source components (2)		
isolate environment					
	vacuum (3)	insulation material (1)	mirror against radiation (2)	equalize internal and external conditions (4)	
prevent internal disturbances					
	isolate heat sources (3)	use heat efficiently (2)	unwanted heat sources outside (4)	avoid direct contact with PCM (1)	
determine PCM pouch heat accumulation	DH = f(rho)	DH = f(melt%)	DH = f(DT)		
	derive from density change (2)	check melt percentage (3)	derive from temperature change (1)		
measure PCM pouch temperature					
	sensors (2)	analogue thermometer (4)	reference material (3)	thermocouples (1)	

figure 3.2 Morphological chart. Numbers in brackets denote the solution order of preference. Only operations of first or second preference qualify for a design combination.

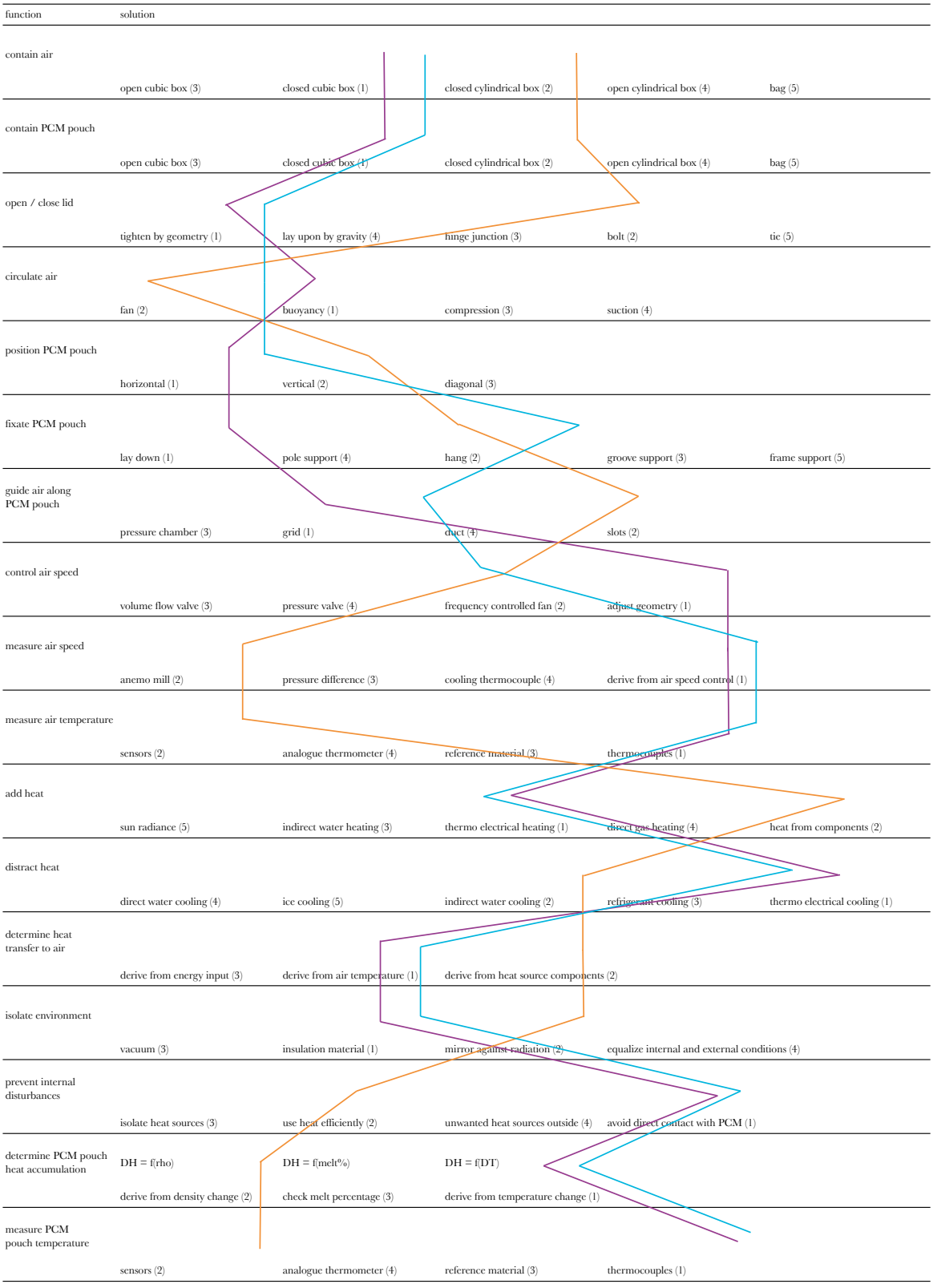

function	solution				
contain air	open cubic box (3)	closed cubic box (1)	closed cylindrical box (2)	open cylindrical box (4)	bag (5)
contain PCM pouch	open cubic box (3)	closed cubic box (1)	closed cylindrical box (2)	open cylindrical box (4)	bag (5)
open / close lid	tighten by geometry (1)	lay upon by gravity (4)	hinge junction (3)	bolt (2)	tie (5)
circulate air	fan (2)	buoyancy (1)	compression (3)	suction (4)	
position PCM pouch	horizontal (1)	vertical (2)	diagonal (3)		
fixate PCM pouch	lay down (1)	pole support (4)	hang (2)	groove support (3)	frame support (5)
guide air along PCM pouch	pressure chamber (3)	grid (1)	duct (4)	slots (2)	
control air speed	volume flow valve (3)	pressure valve (4)	frequency controlled fan (2)	adjust geometry (1)	
measure air speed	anemo mill (2)	pressure difference (3)	cooling thermocouple (4)	derive from air speed control (1)	
measure air temperature	sensors (2)	analogue thermometer (4)	reference material (3)	thermocouples (1)	
add heat	sun radiance (5)	indirect water heating (3)	thermo electrical heating (1)	direct gas heating (4)	heat from components (2)
distract heat	direct water cooling (4)	ice cooling (5)	indirect water cooling (2)	refrigerant cooling (3)	thermo electrical cooling (1)
determine heat transfer to air	derive from energy input (3)	derive from air temperature (1)	derive from heat source components (2)		
isolate environment	vacuum (3)	insulation material (1)	mirror against radiation (2)	equalize internal and external conditions (4)	
prevent internal disturbances	isolate heat sources (3)	use heat efficiently (2)	unwanted heat sources outside (4)	avoid direct contact with PCM (1)	
determine PCM pouch heat accumulation	DH = f(rho) derive from density change (2)	DH = f(melt%) check melt percentage (3)	DH = f(DT) derive from temperature change (1)		
measure PCM pouch temperature	sensors (2)	analogue thermometer (4)	reference material (3)	thermocouples (1)	

figure 3.3 *Morphological chart showing three operational combinations; the purple line connects the solutions of first order preference, the orange line connects the solutions of second order preference, and the blue line is a combination of both.*

To select the final design structure the three operational combinations are rated according to the variable and desirable conditions as mentioned in the schedule of requirements. All three combinations always need to satisfy the fixed requirements. Scores may vary from one to three points. The "blue" combination reaches the highest score of 88% (table 3.) hence it specifies the final design structure.

table 3.2 *Rating of operational combinations. Scores from 0 to 3 are assigned by variable and desirable conditions. The cumulative score equals the score relative to the maximum score, in case every condition would be given 3 points. The purple combination yields 79%, the orange combination yields 64% and the blue combination yields 88% cumulative.*

requirement	score:	0	1	2	3	0	1	2	3	0	1	2	3
PCM pouch length: L ≤ 1000 [mm]		3				1				3			
PCM pouch width: W ≤ 450 [mm]		3				1				3			
PCM pouch thickness: d ≤ 25 [mm]		3				2				3			
the CC is of cuboidal shape		3				2				3			
heat transfer to the pouch: Q ≤ 200 [W/m²]		3				2				3			
heat transfer from the pouch: Q ≤ 120 [W/m²]		2				2				3			
air temperature: 18 [°C] ≤ θ ≤ 28 [°C] (office hours)		2				2				2			
air relative humidity: 30% ≤ RH ≤ 70% - non controllable		1				1				1			
overall air temperature: 5 [°C] ≤ θ ≤ 50 [°C]		3				3				3			
overall air relative humidity: 10% ≤ RH ≤ 90% - non controllable		2				2				2			
air speed: 0.15 [m/s] ≤ v ≤ 0.25 [m/s]		1				3				3			
	cumulative:	79%				64%				88%			
		0%	33%	66%	100%	0%	33%	66%	100%	0%	33%	66%	100%

3.3 Constructional design

The blue combination as depicted in the morphological chart is the combination of operations by function that satisfies the schedule of requirements yielding the final Capacity Cube design structure. In short, the Capacity Cube (figure 3.4) is a cuboidal box, covered by a shape tight lid. It provides space for a rectangular PCM pouch hanging in horizontal position. Air flows around the pouch to heat up or cool down the PCM. A fan forces the airflow and controls the air speed so that the air circulates through the Capacity Cube while it successively passes a water battery, the circulation fan, an airflow guiding grid and the PCM pouch. The water battery is a water-air heat exchanger which controls the air temperature. The airflow guiding grid forces the air to pass the pouch evenly.

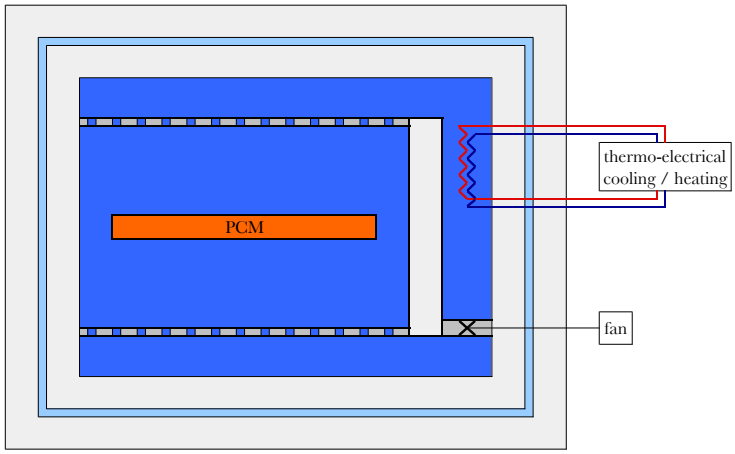

figure 3.4 *Design sketch, front view, of the Capacity Cube resulting from morphological analysis. The part which contains the PCM pouch is referred to as "measuring compartment" whereas the part that controls the air temperature and airflow is referred to as "control compartment".*

This section illustrates the execution of the main functions in more detail. Purpose of the final design is not to manufacture the Capacity Cube but to support the modelling the Capacity Cube. Moreover the final design indirectly supports the PCM pouch modelling. Therefore only the aspects important to the modelling effort are discussed here.

3.3.1 Geometry

Both the PCM pouch dimensions as well as the equipment configuration determine the size of the Capacity Cube. Pouch length and width define the size of the measuring compartment while fan and heat exchanger determine the height of the control compartment. Most likely the maximum applicable pouch thickness will not surpass the aggregate height of fan and heat exchanger. Hence, the height of the control compartment is a measure for the overall height of the Capacity Cube.

The maximum pouch size is approximately 1000 [mm] long by 450 [mm] wide [8]. These measures are enlarged by 50 [mm] on each side to leave enough room for the airflow to pass the PCM pouch (figure 3.5). Air velocities in front of the pouch may vary from 0.15 [m/s] to 0.25 [m/s]. Accounted by the surface ratio of the cross section with pouch over the free cross section, the air velocity through the 50 [mm] strip ranges from 0.44 [m/s] to 0.73 [m/s], which is reasonable.

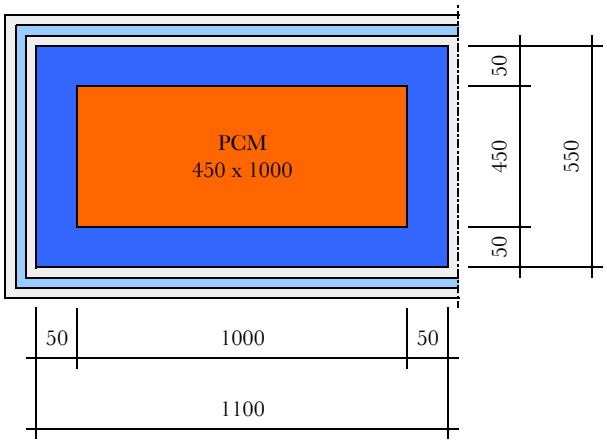

figure 3.5 *Schematic top view of the Capacity Cube measuring room. All dimensions in [mm]. Forced circulating airflow is able to pass the pouch through the strip of 50 [mm] wide on either side of the PCM pouch.*

Since the inside cross sectional area is 1100 x 550 [mm] ≈ 0.61 [m^2], and the air speed ranges from 0.15 [m/s] to 0.25 [m/s], the airflow through the free cross section of the measuring compartment varies between 327 [m^3/h] and 545 [m^3/h]. Companies like Rucon [55], ebm-papst [15], Tombling [66], and others manufacture axial fans with variable speed control. The Capacity Cube applies ebmpapst's axial fan type 5318 (figure 3.6) which controls the airflow between 350 [m^3/h] and 550 [m^3/h] via adjustable voltage input. Corresponding available pressure levels are 620 [Pa] and 440 [Pa] respectively. Its mounting flange is sized 140 x 140 [mm], while its height including housing spans 51 [mm].

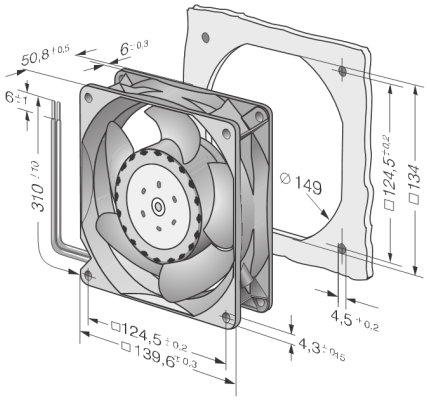

figure 3.6 *Dimensions in [mm] of Ebmpapst axial fan type 5318 [16] as applied by the CC. This type of fan controls the airflow between 350 [m^3/h] (620 [Pa]) and 550 [m^3/h] (440 [Pa]).*

The airflow through the Capacity Cube is either heated up or cooled down by thermo electric modules, which add or remove heat to or from the air stream by imposing a

temperature difference whenever an electrical current is applied. Changing the polarity of the current will reverse the direction of heat transfer. Therefore thermo electrical modules serve as heater or cooler depending on the electrical polarity applied. Moreover multiple elements connected in series will increase the overall cooling or heating capacity.

The Capacity Cube uses four Tetech AC-046 modules (figure 3.7) [63] connected in series to satisfy the cooling requirement of 100 [W] and to satisfy the heating requirement of 200 [W]. Heat sinks of the Tetech AC-046 air to air coolers have metal fins attached to enlarge the heat transfer surface. Additional fans direct air streams through the fins on both the hot and cold side. However, since the Capacity Cube already uses the Embpapst axial fan, the fans on the thermo electrical modules at the inside of the CC are no longer needed. These fans can be removed without losing functionality [64].

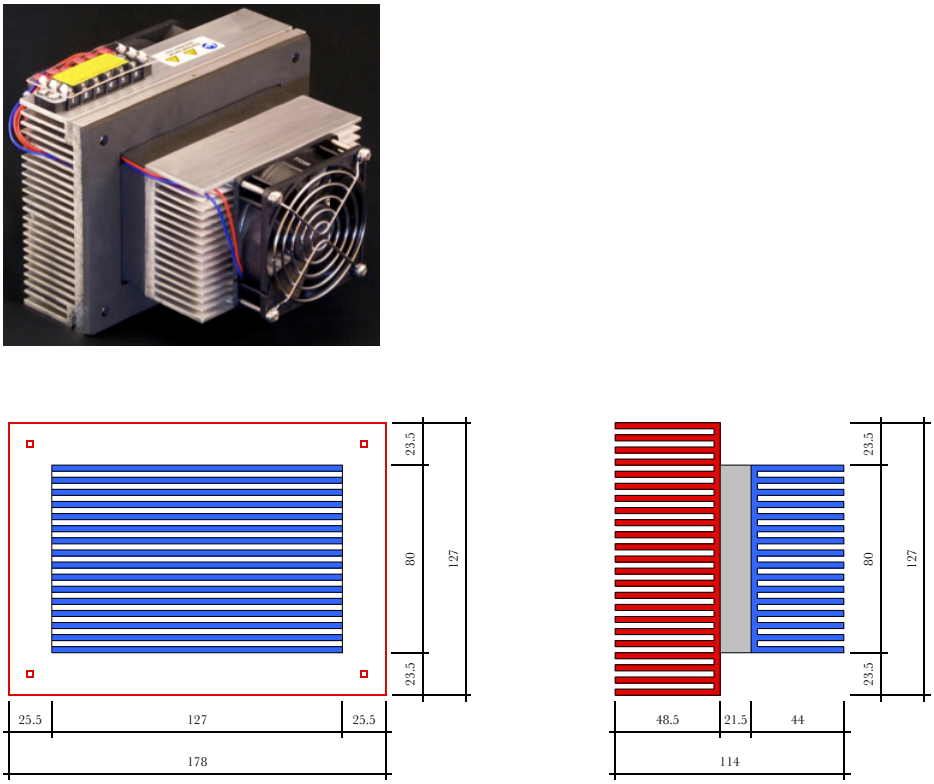

figure 3.7 *Tetech AC-046 thermoelectrical module [63]. The full configuration is shown topmost. Schematically shown below that, are the front view (left) and side view (right), where red and blue coloured parts denote the hot and cold sides of the module. All dimensions in [mm].*

The smaller heat sink of the module cools down the inside air of the Capacity Cube. After reversing the polarity applied to the thermoelectric modules the heat sink will heat up the air instead. The larger part of the module serves as heat exchanger outside the Capacity Cube. Inside the Capacity Cube each module is 80 [mm] wide and 127 [mm] high, whereas outside the Capacity Cube each module is 127 [mm] wide by 178 [mm] high.

Hence, four modules adjacent outside the Capacity Cube span a total width of 508 [mm] whereas inside the Capacity Cube the modules spread with a 47 [mm] pitch.

3.3.2 Control

The Capacity Cube controls the PCM temperature and the surrounding air temperature by varying the heat load of the thermoelectrical module. Cooling and heating rates of the modules are proportional to the electrical power input. Reducing the power input will reduce the rate of heating or cooling and vice versa. Temperature transmitters (figure 3.8) with an accuracy of ± 0.1 [K] provide the signal required to adapt the electrical power input to the modules.

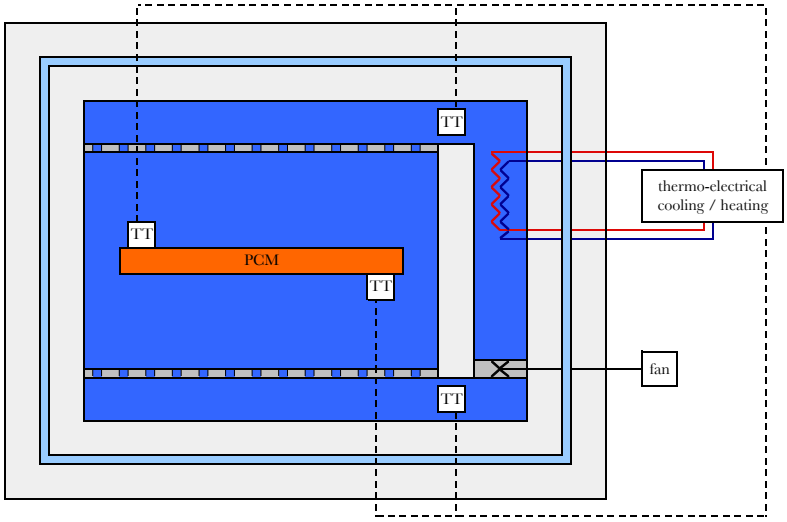

figure 3.8 *Capacity Cube control lay out. Temperature transmitters (TT) measure the air temperature and PCM surface temperature and provide the signal (---) to control the heating or cooling rate applied by the thermoelectric modules.*

3.3.3 Material

When choosing the appropriate materials to build up the Capacity Cube three aspects are important. At first the materials need to be thermal insulators to minimize heat transfer between the Capacity Cube and its surroundings. Secondly, the materials should be sufficiently rigid and strong to support the PCM pouches as well as the fan and thermoelectric modules. And third, the materials have to comply with the conditions stated by the schedule of requirements.

The body of the Capacity Cube is comparable to a small aquarium, consisting of a glass container with a wall thickness of 4 [mm]. On the inside and outside a 100 [mm] thick layer of expanded polystyreen insulation material covers the glass walls of the container. Such a wall composition (figure 3.9) not only keeps the container airtight, but also limits heat exhange with the surroundings.

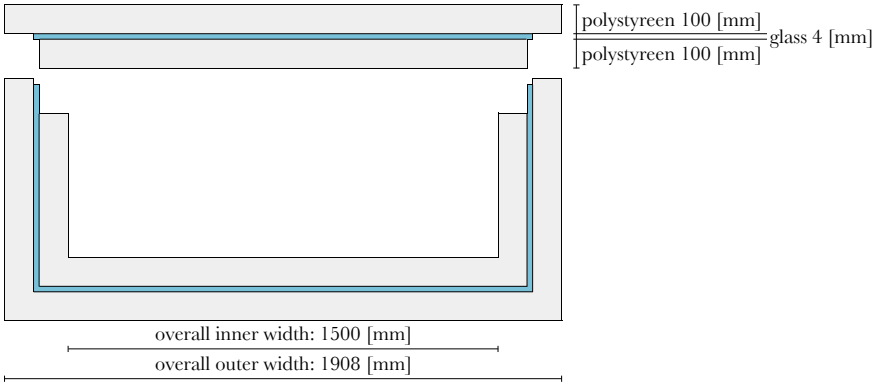

figure 3.9 *Capacity Cube envelope with the lid separated. The outer walls consist of three layers; two polystyreen layers of 100 [mm] and a 4 [mm] glass layer.*

Besides its relatively low thermal conductivity, expanded polystyreen retains its shape when exposed to temperatures up to 80 [°C] [67, 68]. Moreover the material is relatively easy to process, which makes it useful to put together the Capacity Cube. Expanded polystyreen also supports the lightweight grids that guide the airflow along the PCM pouch. Since these polypropylene grids (figure 3.10) are a mere 1.6 [mm] thick [45] their specific heats are minimized in relation to the specific heat of the PCM pouch.

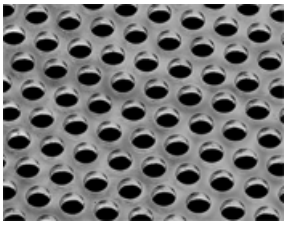

figure 3.10 *Polypropylene grid [45] to guide the airflow from bottom to top, along the PCM pouch, through the Capacity Cube. The hole diameters and hole pitches are approximately 5 [mm] and 8 [mm] respectively. 32% of the grid is open surface.*

3.3.4 Design layout

Now all relevant parts are addressed, the combination of components issues the Capacity Cube design layout (figure 3.11a and 3.11b). The final design aspires compactness for efficient use of space and to prevent loss of functionality. Operational aspects are the subject of the next chapter.

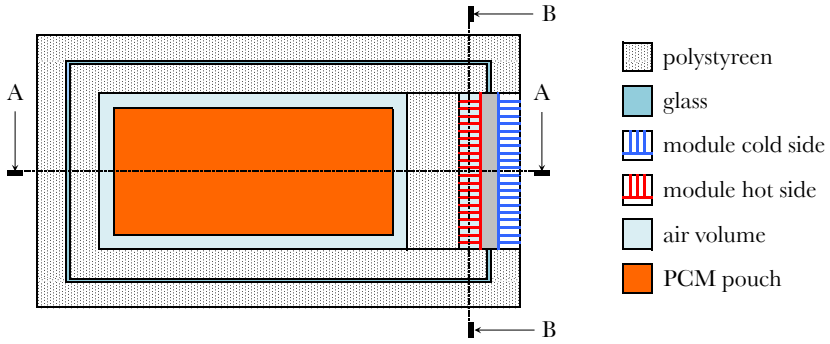

figure 3.11a Capacity Cube design layout. This top view indicates the cross sections for front view (figure 3.11b) and side view (figure 3.11c). Also shown is the legend clarifying the materials and components.

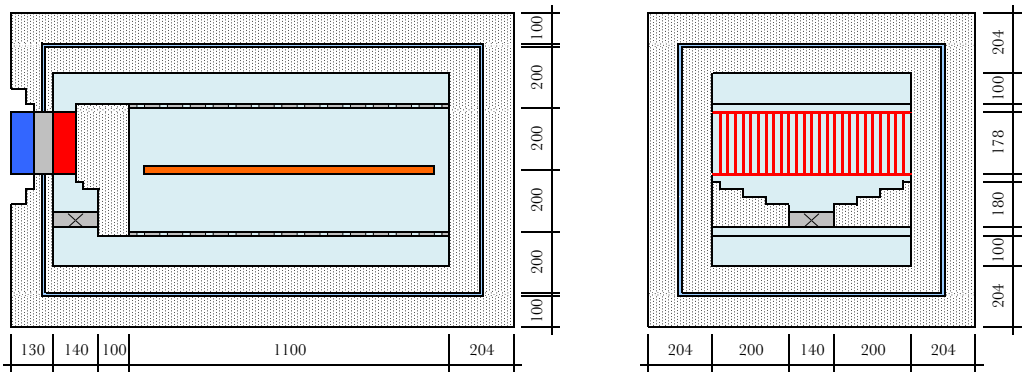

figure 3.12b Capacity Cube design layout (continued). The side view (left) and front view (right) show cross sections A-A and B-B (figure 3.11a/b) with selected dimensions in [mm].

4 CAPACITY CUBE MODEL

Fundamental modelling concepts for both scientific and engineering purposes have been published by Golomb [23], Kwatny and Mablekos [41], and Willems [69], amongst others. Bosgra [5] gives a comprehensive overview by presenting a modelling method common for engineering purposes, which comprises the following aspects:

a) purpose
b) system border and variables
c) relevant phenomena
d) hypotheses
e) sub models
f) conservation laws and constitutive equations
g) implementation
h) validation and application

Together with the explanation of system border and variables the model purpose concludes the model definition (4.1). Further, both the relevant phenomena and hypotheses yield the physical model representation (4.2). The structure of the Capacity Cube model becomes clear from the sub model division and mathematical composition (4.3). Finally, the implementation of equations gives the model results, which are then validated and evaluated (4.4).

4.1 Model definition

The Capacity Cube envelope encloses the two compartments that contain the PCM pouch on the one hand and hold the thermoelectric module and fan assembly on the other hand. Although heat transfer between the two compartments cannot be ruled out completely the Capacity Cube model focuses on the compartment that includes the PCM pouch. Note that the PCM pouch is not yet part of the model. The PCM pouch model is the subject of the next chapter. This section focuses on the Capacity Cube model only.

4.1.1 Purpose

Purpose of the model is to simulate heat flows within the Capacity Cube and to simulate heat flows from the Capacity Cube to the surroundings. Moreover air temperatures at different locations throughout the Capacity Cube are investigated. Eventually the Capacity Cube model will be used to implement the PCM pouch model and analyze the PCM pouch behaviour.

4.1.2 System border

The Capacity Cube compartment that contains both the thermoelectric module and the fan controls the heat and cooling loads as well as the air supply volume flow. On the contrary, the compartment that holds the PCM pouch measures air temperatures and provides the necessary control signals. Therefore the latter compartment is considered the system whereas the control compartment is part of the surroundings (figure 4.1). The system boundary crosses the adiabatic wall between the two compartments as well as it crosses the air supply and air return openings. Furthermore the system boundary matches the Capacity Cube envelope.

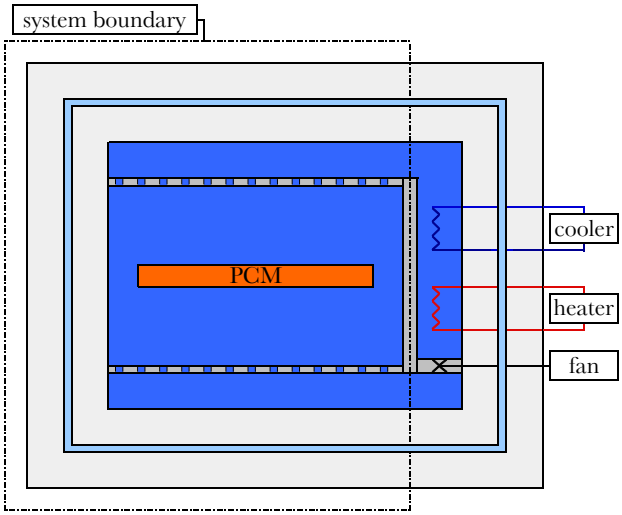

figure 4.1 *The system boundary defines the compartment containing the PCM pouch including the accompanying envelope (system) in its interior contrary to the exterior of environmental air and the compartment holding the thermoelectrical modules and air displacement fan (surroundings).*

4.1.3 Variables

Input variables originate in the surroundings whereafter they act upon the system. Input variables influence the system by passing the system boundaries inwards. Vector x(t) contains the input variables:

$$x(t) = \begin{bmatrix} T_{in} & T_{out} \end{bmatrix} \tag{4.1}$$

Variables that result from relations within the system are called output variables. Output variables become available to the surroundings by passing the system boundary outwards. Vector y(t) contains the output variables:

$$y(t) = \begin{bmatrix} Q_{in} & Q_{out} \end{bmatrix} \tag{4.2}$$

Internal variables are variables that are present within the system but they do not belong to the input variables. To distinguish between input and output variables the internal variables are referred to as parameters. Vector z(t) contains the parameters:

$$z(t) = \begin{bmatrix} L & W & H & d & \rho & c_p & v & \lambda & \alpha_C & \alpha_D & \alpha_R \end{bmatrix} \tag{4.3}$$

Note that input and output variables in terms of temperature and heat flow are bilaterally coupled. Hence, they cannot be imposed simultaneously. Temperature inputs result in heat flow outputs and vice versa. Moreover the input and output variables are marked with indices that represent the entering (in) and leaving (out) variables relative to the system. Entering variables do not need to be system input variables and leaving variables are not necessarily system output variables. The internal variables are geometry parameters, material properties, air velocity and heat transfer coefficients.

4.2 Physical model representation

Explanation of the relevant phenomena together with the statement of hypotheses and assumptions represent the Capacity Cube model in concept. First the phenomena describe the physical processes relevant to the use of the model. Then the hypotheses and assumptions simplify these underlying process physics.

4.2.1 Relevant phenomena

Since the model simulates temperature levels related to the applied heat loads, the relevant phenomena include heat flow and heat storage instances. Moreover air is the heat transfer medium between the two rooms of the Capacity Cube, hence the airflow is also taken into account:

1) air is forced to flow from the fan to the bottom part of the Capacity Cube, initially in horizontal direction as the bottom wall and horizontal grid enclose the airflow. Further the grid guides the airflow in vertical direction to the upper side of the Capacity Cube. Finally the second grid at the top side guides the airflow in horizontal direction back to the fan, similar to the bottom side.
2) convective heat transfer between airflow and inner walls
3) convective heat transfer between airflow and air guiding grids
4) conductive heat transfer within the envelope walls
5) radiative heat transfer between mutual inner walls
6) radiative heat transfer between outer walls and surroundings
7) energy accumulation within air volumes
8) energy accumulation within air guidance grids
9) energy accumulation within envelope walls

4.2.2 Hypotheses and assumptions

The physics of the real processes are simplified by the hypotheses and assumptions. Model properties are adapted to the specific situation of application by which the model validity reduces but its simplicity increases. Following hypotheses and assumptions are singled out:

a) Lumped model approach. Spatial distributions are not of interest. Control volumes are considered ideally mixed. Consequently variables have identical values over the total volume.
b) No moving boundaries. Control volumes, i.e. wall volumes and air volumes, are time invariant. In practice control volumes expand or contract due to density and temperature variations, however these volume changes are negligible when accounting heat transfer effects.
c) No work done by or on the airflow. Forces acting on the Capacity Cube walls and pressure variations caused by the airflow as well as displacements of the system boundary hardly affect the conductive, radiative, or convective heat transfer modes.

d) Changes in potential and kinetic energy of the control volumes are negligible since both height differences and air velocity changes are relatively small.
e) Material properties are constant, except for air properties. The Capacity Cube envelope consists of solid walls. The applicable temperature range is approximately 5 [°C] to 55 [°C]. Solid wall physical properties hardly change within the temperature range. However air properties, such as density and viscosity, vary with temperature.
f) Heat transfer coefficients either depend on air velocity (convection) or on surface view factor (radiation) only, since heat transfer coefficients are weak functions of temperature (see appendices).
g) No condensation or other phase changes occur within the Capacity Cube. Atmospheric pressure prevails and temperature levels remain well above air saturation conditions.

In the next section the Capacity Cube is divided into subsystems. Though the hypotheses and assumptions refer to the cube in general, they also hold for distinct submodels.

4.3 Model structure

The model divides the Capacity Cube into twenty-seven nodes. Besides, to distinguish between horizontal and vertical walls, the Capacity Cube consists of four regions A to D (figure 4.2). Note that the PCM pouch is already labeled for future purposes only, it is not yet part of the model.

Each node designates a particular part of the Capacity Cube, e.g. nodes 1, 9, 15 and 21 represent air volumes "A" to "D" respectively, and nodes 8 and 20 represent the grids that guide the airflow. Heat transfer modes between the nodes are denoted by a single letter, where C means convection, D means conduction, R means radiation and F stands for airflow. The nodes and heat transfer modes serve as the submodels that compile the total Capacity Cube model. Storage modules account for the energy accumulation within the nodes whereas resistive modules account for the energy transfer between the nodes.

To all submodels, either storage or resistive, the energy conservation equation applies. A set of independent equations remains after substitution of mathematical simplifications corresponding to the hypotheses and assumptions. Since the number of unknown variables equals the number of independent equations, the unknowns to all submodels are calculated by solving the remaining set of equations.

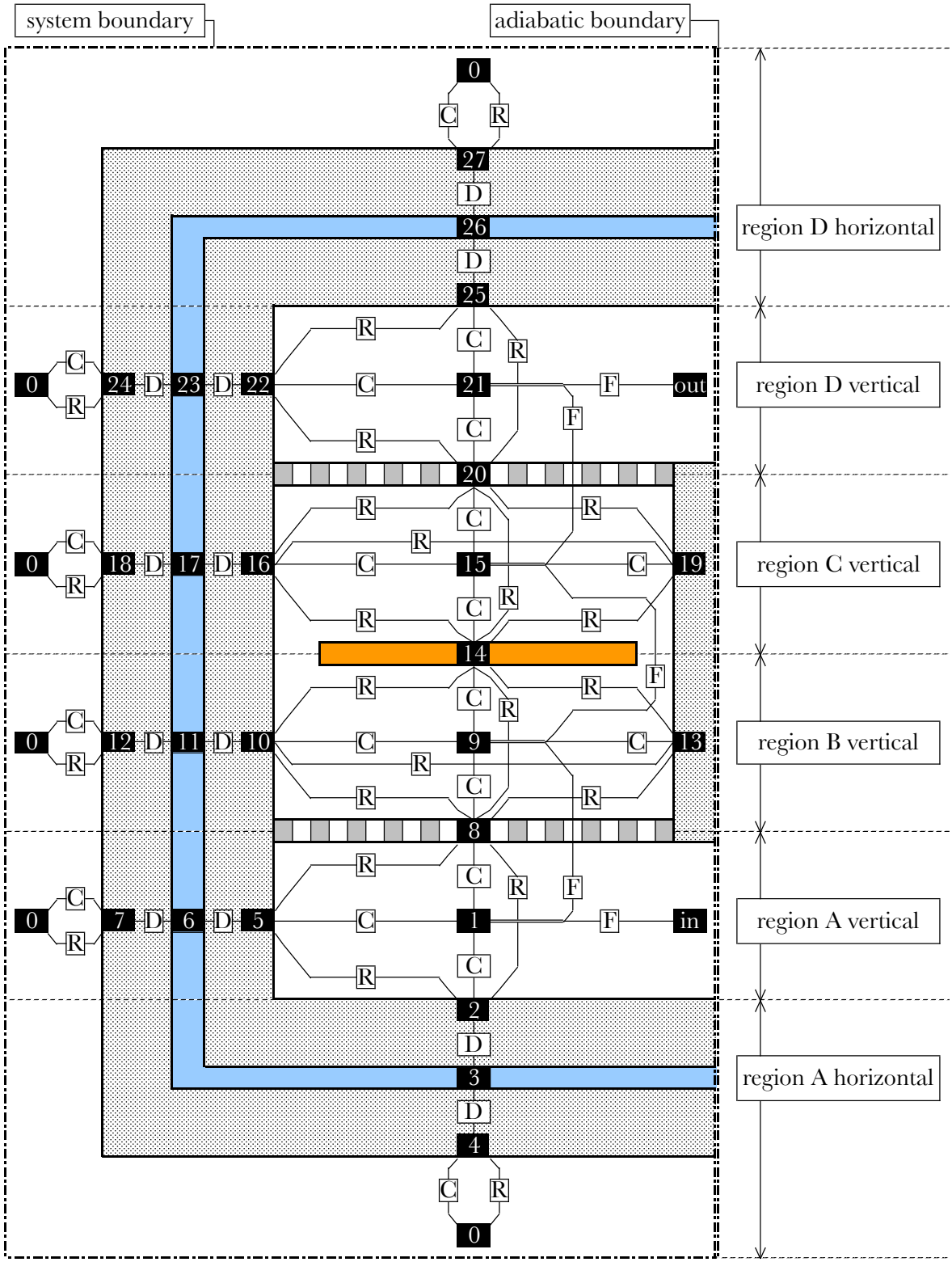

figure 4.2 *Capacity Cube nodal model setup. Black numbered blocks represent the nodes. White lettered blocks represent the heat transfer modes, where C means convection, D means conduction, R means radiation and F stands for airflow.*

4.3.1 Submodels

All four regions A to D consist of resistive modules that represent the heat transfer modes and storage modules that represent the physical nodes (figure 4.3). For convenience only region A is shown. Regions B, C and D are similarly modelled.

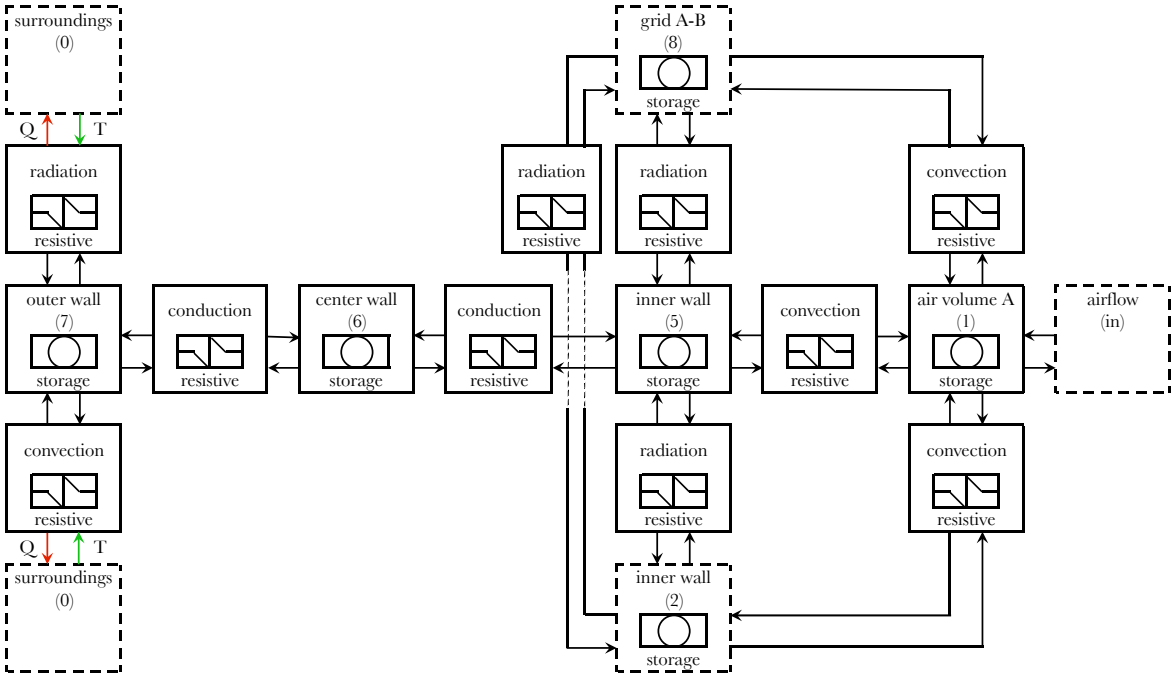

figure 4.3 *Overview of resistive and storage submodels for region A. Regions B, C and D are not shown because these regions are identical in modelling terms. Dashed contour blocks denote the nodes where region A connects to either the surroundings or to one of the three other regions. Red arrows stand for model output variables and green arrows stand for model input variables. Resistive modules account for heat transfer effects while storage modules account for the energy accumulation within the nodes. Numbers in parentheses correspond to node numbers in the full model.*

A closer look at the modules around node 7, the outer vertical wall of region A, show that the node itself is a storage module which accumulates heat (figure 4.4). Three resistive modules attach to the storage module. The conduction module accounts for heat transfer by conduction between the outer vertical wall and the center vertical wall. The other resistive modules represent heat transfer with the surroundings.

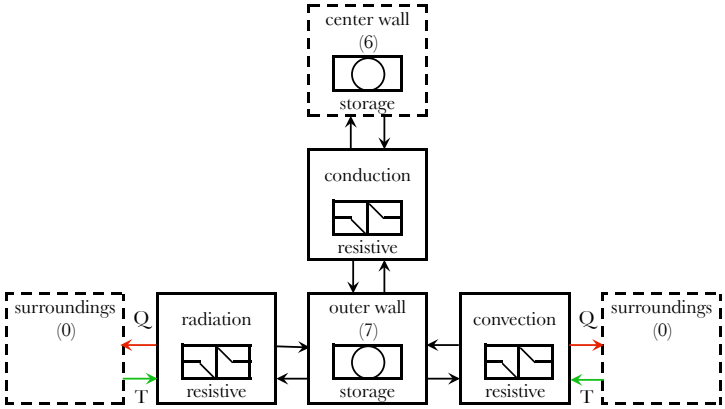

figure 4.4 *Detail of submodelling node 7, the outer vertical wall from region A. The scheme is rotated 90° counterclockwise with respect to figure 4.3. Outer vertical wall A transfers heat with the surroundings by convection and radiation, whereas it transfers energy by conduction with the center wall of region A.*

Although heat transfer modes are shown distinctively in the figures above, most often they coexist or they directly follow up each other. For example, convective and radiative heat transfer between outer vertical wall A and its surroundings act simultaneous. Therefore, analogue to resistances in electrical circuits, such coexisting or subsequent heat transfer modes are regarded as single resistive modules, and summed up correspondingly.

4.3.2 Conservation laws and constitutive equations

From the hypotheses and assumptions follows that mass conservation equation is not required to describe the phenomena encountered by the Capacity Cube envelope walls. However the mass conservation equation does apply to the distinct air volumes:

$$\frac{dm}{dt} = f_{in} - f_{out} \tag{4.1}$$

Moreover the energy conservation equation applies:

$$\frac{dE}{dt} = Q_{in} - Q_{out} \tag{4.2}$$

Where the energy accumulation within a particular node is given by:

$$\frac{dE}{dt} = \frac{d}{dt}\left(mc_pT\right) \tag{4.3}$$

Material properties apart from air properties are assumed constant, and volumes are time invariant. Furthermore the model utilizes backward differentiation to increase stability. Therefore the discretisation of energy accumulation with respect to time becomes:

$$\frac{d}{dt}\left(mc_P T\right) = mc_P \frac{T^j - T^{j-1}}{\Delta t} \tag{4.4}$$

Since air specific mass varies with time, also the masses of the nodes that represent air volumes vary with time. Hence the energy accumulation discretisation for the nodes that represent air volumes yields:

$$\frac{d\left(mc_P T\right)}{dt} = T^{j-1}c_P \frac{m^j - m^{j-1}}{\Delta t} + m^{j-1}c_P \frac{T^j - T^{j-1}}{\Delta t} \tag{4.5}$$

In equation (4.3) the entering and leaving heat rates are defined by the heat transfer equations of convection, conduction and radiation [33, 35], see also appendices A and C:

convection: $$Q_C = \alpha_C A \Delta T \tag{4.6}$$

conduction: $$Q_D = \alpha_D A \Delta T \tag{4.7}$$

radiation: $$Q_R = \alpha_R A \Delta T \tag{4.8}$$

Besides, for the heat transfer associated with airflow holds:

$$Q_F = \varphi \rho c_p \Delta T \tag{4.9}$$

Analogue to the total equivalent of resistances in series or parallel resistances in an electrical current network, the overall heat transfer rate reciprocally relates parallel and serial heat transfer modes:

serial heat transfer: $$Q = \frac{A}{\alpha_C^{-1} + \alpha_D^{-1} + \alpha_R^{-1}} \Delta T \tag{4.10}$$

parallel heat transfer: $$Q = \frac{A}{\left(\alpha_C + \alpha_D + \alpha_R\right)^{-1}} \Delta T \tag{4.11}$$

4.4 Model implementation

The last step in the modelling process issues the Capacity Cube model. Execution of the model focuses on validating the model outputs. The chapter is concluded by a discussion on the model applicability.

4.4.1 Validation

Since the Capacity Cube is newly designed, there are no actual measurements to compare the model results with. However its phenomenal behaviour is verified by qualitative validation to ensure further experimental usage. The validation comprises a temperature step input and a heat rate step input. In both cases the temperature response of the air volumes is considered.

While the surrounding air temperature remains 20 [°C] two temperature steps are applied; an increasing temperature input from 20 [°C] to 25 [°C] and a decreasing temperature input from 30 [°C] to 10 [°C]. The air volume temperatures are expected to follow the input temperature, where the air temperatures will asymptotically reach but not surpass the final inside temperature. Model outputs support the expected behaviour (figure 4.5).

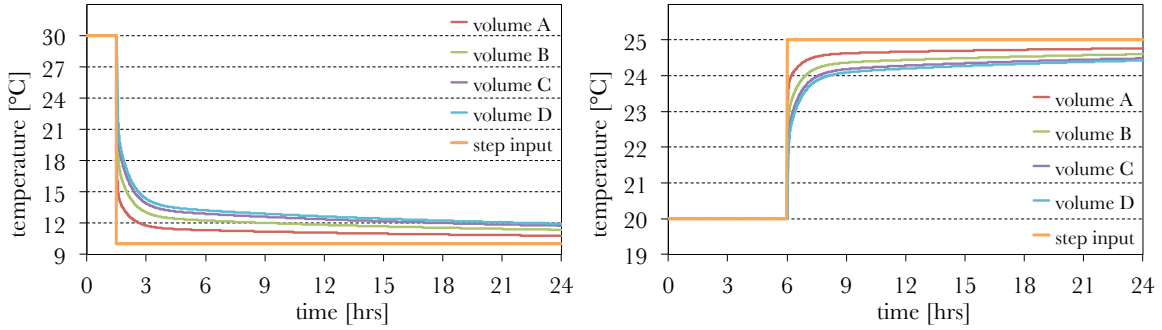

figure 4.5 *Capacity Cube validation by imposing a temperature step input from 30 [°C] to 10 [°C] (left) and a temperature step input from 20 [°C] to 25 [°C] (right). Air volume temperature responses are delayed because of accumulation effects. Moreover heat losses to the surroundings cause the air volume temperatures to reach the input temperature asymptotically.*

The air volume temperatures will respond in a similar fashion to heat rate steps as to temperature steps. But heat losses to the surroundings are relatively small, so constant heat inputs will cause the air temperatures to rise over time instead of flatten out and approach to the input load. Indeed, air temperature responses satisfy the expectations for an 80 [W] step down and an 80 [W] step up heat input respectively (figure 4.6).

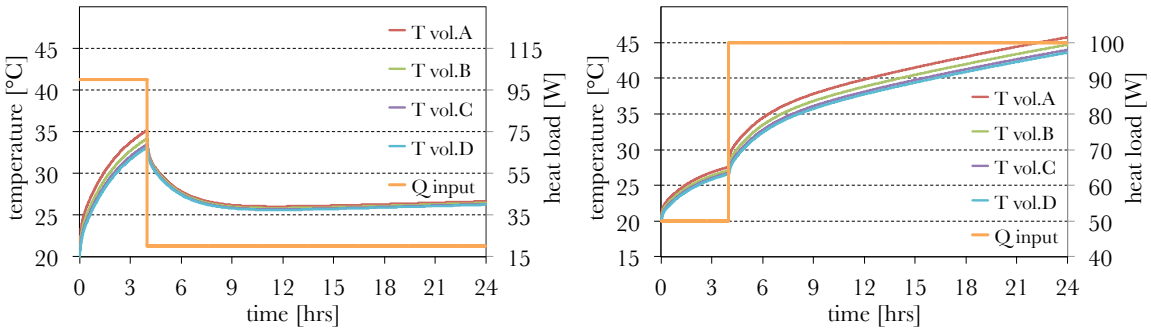

figure 4.6 *Capacity Cube validation by imposing an heat load step up from 100 [W] to 20 [W] (left) and an heat load step down from 20 [W] to 100 [W] (right). Initial air temperatures are set to 20 [°C]. Constant heat loads cause air temperatures to increase, however responses delay because of accumulation effects.*

4.4.2 Discussion

Air velocities are high compared to the characteristic control volume dimensions. For air velocities varying between 0.1 [m/s] and 0.3 [m/s] the typical air change rates range from 0.5 to 3 times per second. Therefore energy accumulation effects within the air volumes are small with respect to the heat exchange effects and the model runs by small time steps only. Consequently, the daytime simulation of 24 [h] corresponds with a single hour real time simulation.

Convective heat transfer coefficients between grids and airflow are determined according to correlations by Sparrow and Carranco Ortiz [60], see also appendix B. The correlations hold when the ratio of pitch over hole diameter equals 2.0 to 2.5. However, the grids in the Capacity Cube yield approximately a pitch over hole ratio of 1.5. Moreover the heat convection coefficients around the grids are about ten times as large as the convection coefficients at the walls and at least three times as large as the convection coefficients at the pouch. To prevent frustration of the model stability the convective heat transfer coefficients between grids and airflow are assumed equal to the heat convection coefficients at the pouch.

Air volume D is the topmost compartment of the Capacity Cube. Its temperature depends on the entering and leaving heat rates to or from the node. Since the volume is represented by the last node in series (node 21), its leaving heat rate by airflow is unknown. Therefore volume D is partially modelled as heat sink. Heat rates from the node to the envelope walls are taken into account, but heat transfer associated with leaving airflow is neglected. The model thus provides a temperature of volume D which is higher than its actual value. However a symmetry analysis based on proportional temperatures of volumes A and B figures that the error introduced is less than 2%.

5 PCM POUCH MODEL

This chapter presents a dynamic model of PCM pouches in general. The modelling method [5] followed here is common in engineering sciences and involves the features as previously introduced in chapter 4.

Section 5.1 addresses purpose, system border and variables to define the model. Section 5.2 describes the relevant phenomena and hypotheses which represent and simplify the physical processes. Section 5.3 clarifies the model structure through division of the PCM pouch into submodels and through formulation of the mathematical equations. Section 5.4 implements the equations, validates the model and discusses the results.

5.1 Model definition

The Capacity Cube holds the PCM pouches in horizontal position, perpendicular to the flow direction. Air is flowing from bottom to top along the sides of the pouch. Although the Capacity Cube encloses the PCM surroundings and the airflow cannot be omitted, the intention is to define the PCM pouch model as general as possible, without disregard of the modelling conventions.

5.1.1 Purpose

Purpose of the model is to simulate the temperature gradient within the PCM pouch as a function of the applied heat load. Moreover the PCM energy storage capacity throughout phase change is investigated. Eventually the PCM pouch model will be used in the Capacity Cube model to analyze the behaviour of different PCMs during their phase transitions.

5.1.2 System border

The PCM pouch is considered the system (figure 5.1). The system boundary matches the PCM pouch outer surface. The airflow around the pouch coupled with the Capacity Cube envelope represents the surroundings.

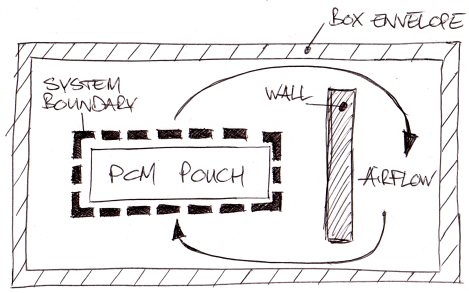

figure 5.1 *The system boundary defines the PCM pouch (system) in its interior contrary to the exterior of airflow and Capacity Cube envelope (surroundings).*

5.1.3 Variables

Variables are previously discussed in chapter 4, section 4.1.3. General definitions for input, output and internal variables applicable to the Capacity Cube model also hold for the PCM pouch model. For completion only the vectors are given here.

input variables: $$x(t) = \begin{bmatrix} T_{in} & T_{out} \end{bmatrix} \quad (5.1)$$

output variables: $$y(t) = \begin{bmatrix} Q_{in} & Q_{out} \end{bmatrix} \quad (5.2)$$

parameters: $$z(t) = \begin{bmatrix} L & W & H & \rho & \lambda & \alpha_C & \alpha_D & \alpha_R \end{bmatrix} \quad (5.3)$$

5.2 Physical model representation

Physical processes relevant to the use of the model are paraphrased in relevant phenomena. Then hypotheses and assumptions simplify these process physics. Together the phenomena, hypotheses and assumptions conceptually represent the PCM pouch model.

5.2.1 Relevant phenomena

As the model simulates the PCM heat storage capacity and the temperature gradient within the pouch regarding the heat load applied, the relevant phenomena mainly comprise heat flow and heat storage behaviour. Since the PCM surrounding air temperature is the driving force for heating and cooling the pouch, the airflow is considered as well:

1) air flows from bottom to top passing alongside the pouch
2) convective heat transfer between airflow and PCM
3) radiative heat transfer between PCM and surrounding walls
4) conductive heat transfer within the PCM pouch
5) energy accumulation within the PCM

5.2.2 Hypotheses and assumptions

Hypotheses and assumptions replace the process physics in a simplified way. By adapting the model properties to the specific situation in which the model is applied, the validity of the model is reduced, yet the model simplicity is increased. The following hypotheses and assumptions are distinguished:

a) No moving boundaries. The PCM pouch volume is time invariant. In practice the pouch expands or contracts due to density variations as a function of temperature, however these volume changes are negligible when accounting heat transfer effects.
b) No work done by or on the pouch. Forces acting on the pouch and pressure variations caused by the airflow as well as displacements of the system boundary hardly affect the conductive, radiative, or convective heat transfer modes.
c) No PCM mass flow within the pouch. The thickness of the pouch is much smaller than its width and length, and the airflow is evenly distributed over the pouch cross section, hence heat transfer rates due to internal convection are negligible compared to conductive heat transfer rates.
d) Lumped model approach. Spatial distributions are not of interest. The control volume is considered ideally mixed. Consequently PCM particles are indistinguishable. Variables have identical values over the elements contained by the total volume.
e) Radiation configuration factors between pouch and surrounding walls equal unity. Heat radiation between pouch and surrounding walls

depends on the local temperature difference. It is assumed that the pouch is fully surrounded by wall surfaces.

f) The PCM specific heat is a rectangle function of temperature. The specific heat of solid PCM approximately equals the specific heat of liquid PCM. During phase change the specific heat is much higher. By assumption the PCM phase transition occurs at a small temperature range where the specific heat reaches a peak value.

In the next section the PCM pouch is not longer regarded as a single body to model, different layers are specified instead. Though the hypotheses and assumptions refer to the pouch, they also hold for distinct layers.

5.3 Model structure

The model divides the PCM pouch into ten layers of equal thickness. Layer 1 is the bottom layer which comes in contact with the airflow first. Layers are numbered in direction of the airflow; layer 10 is the top layer of the pouch. Each layer specifies submodels by means of resistive and storage modules. Resistive modules represent the heat transfer modes whereas storage modules represent energy accumulation phenomena. To all submodels, either resistive or storage modules, the energy conservation applies. By substitution of the mathematical simplifications that correspond with the hypotheses and assumptions a set of independent equations remains. Because the number of independent equations equals the number of unknown variables, all unknowns are determined for each submodel by solving the equation set.

5.3.1 Submodels

Submodels distinguish between resistive and storage modules. All ten layers consist of resistive and storage modules (figure 5.2). For convenience only layers 1 and 2 and layers 9 and 10 are shown. Layers 3 to 8 are left out since layers 2 to 9 are identical in modelling terms.

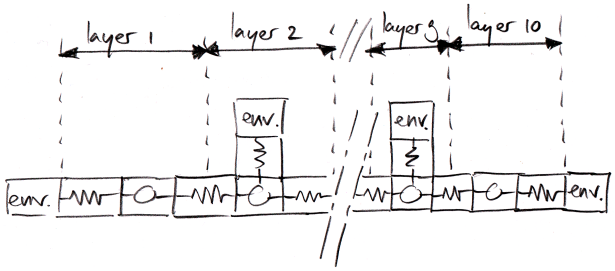

figure 5.2 *Overview of the PCM pouch divided into ten layers that consist of resistive and storage sub models. Layers 3 to 8 are left out for these layers are similar to layers 2 and 9.*

Let us have a closer look at the modules of layer 1 (figure 5.3). The storage module represents the PCM core of the layer which accumulates energy. Two resistive modules attach to the storage module. These modules represent the heat transfer modes of the layer. The PCM layer transfers heat by convection with the surroundings because of the forced airflow that passes alongside the layer. Moreover radiative heat transfer occurs in consequence of the temperature difference between layer and surrounding surfaces. The third resistive sub model accounts for the heat conduction within the layer.

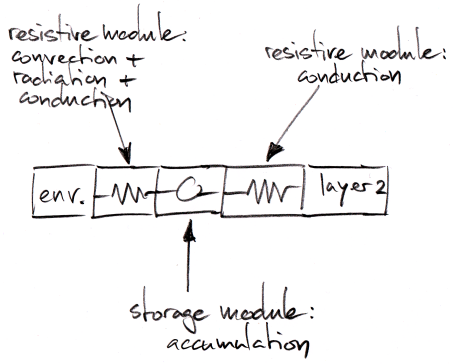

figure 5.3 *Sub modelling bottom layer 1. From left to right; convection, radiation and conduction between the layer and its surroundings (left), accumulation within the layer (center) and conduction between the layer and the adjacent layer (right).*

In practice the heat transfer modes follow up or occur simultaneously. For example, the bottom surface of layer 1 transfers energy by radiation with the surrounding surfaces. At the same time the air is flowing along the layer's surface causing a convection term. Then heat conduction from the surface to the layer's core follows up both radiative and convective heat transfer modes. Therefore simultaneous or consecutive heat transfer modes are modelled as single resistive modules.

5.3.2 Conservation laws and constitutive equations

Energy conservation, mass conservation and momentum conservation are the fundamental conservation laws. However the hypotheses and assumptions state that no PCM mass transfers within the pouch or within a particular layer, hence the mass conservation and momentum conservation equations are not needed to describe the physical phenomena encountered by the pouch. The energy conservation equation yields:

$$\frac{dE}{dt} = Q_{in} - Q_{out} \tag{5.4}$$

The basic equations of heat transfer by radiation, conduction and convection prescribe the entering and leaving heat rates (equations (4.6) to (4.8). In addition to equation (5.4) the accumulated amount of energy within the PCM layer is given by:

$$\frac{dE}{dt} = \frac{d}{dt}\left(mh\right) \tag{5.5}$$

PCM enthalpy changes are defined as:

$$dh = \int c_P\left(T\right)dT \tag{5.6}$$

Boundaries are non-moving, volumes are time invariant and there is no massflow within the pouch layers. Moreover time dependent variables are calculated by backward differentiation. Hence, after substitution, time discretisation of the energy accumulation equation becomes:

$$\frac{d}{dt}\left(mh\right) = m\frac{h^{j} - h^{j-1}}{\Delta t} = mc_P^{j}\frac{T^{j} - T^{j-1}}{\Delta t} \tag{5.7}$$

Where superscripts j and j-1 express two successive time steps. The specific heat at any instant j is approximated by the rectangle function:

$$c_p^{j} = \begin{cases} c_{p,sol} & \text{if} \quad T^{j} < T_{pc} \\ c_{p,pc} & \text{if} \quad T^{j} = T_{pc} \\ c_{p,liq} & \text{if} \quad T^{j} > T_{pc} \end{cases} \tag{5.8}$$

5.4 Model implementation

As final stage to the modelling process, application of the PCM pouch model concentrates on validating the model output values. Validation includes qualitative as well as quantitative validation. A brief discussion on the pouch model concludes this section.

5.4.1 Quantitative validation

Quantitative validation involves the comparison of theoretical model outputs with results obtained in practice, e.g. as an outcome of experiments by physical measurements. Here, the PCM pouch model results are compared to outputs that Bouwman generated with the water bath method [6]. Since the water bath contains live size PCM pouches, these experiments are similar to the effort of modelling the PCM pouch, especially when the water bath parameters are adapted (table 5.1).

table 5.1 *Water bath parameters [6, 8] required to match the measurements with the PCM pouch model. Note that the water bath method carries out measurements on two pouches which are tied together. The applied pouch thickness is therefore twice the thickness of a single pouch.*

property	value	units
pouch length	300	[mm]
pouch width	80	[mm]
pouch height (thickness)	10	[mm]
PCM specific mass	1450	[kg/m^3]
PCM heat conductivity	0.7	[W/mK]
PCM specific heat	3.7	[kJ/kgK]
PCM heat of fusion	110	[kJ/kg]
convective heat transfer coefficient	200	[W/m^{2}K]

During a continuous heating test Climsel C22 PCM pouches [8] were surrounded by water which temperature increased at a rate of about 2.9 [K/h]. While running the experiment Bouwman recorded water and pouch temperatures (figure 5.4, left). When imposing an identical water temperature rate at the PCM model, the pouch temperature evolves likewise (figure 5.4, right).

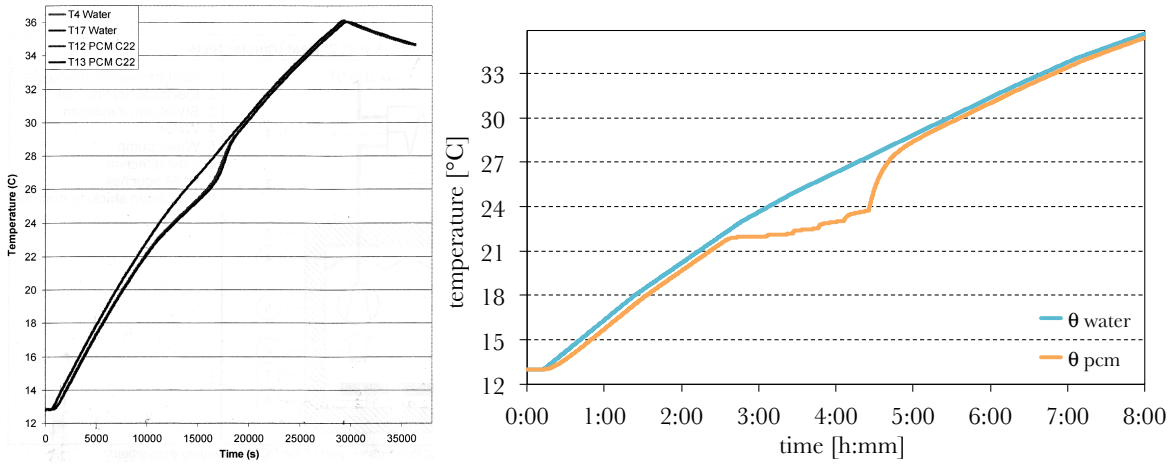

figure 5.4 *Quantitative validation of the PCM pouch model. Measured temperature rates (left) correspond to the modelled temperature rates (right).*

5.4.2 Qualitative validation

Contrary to quantitative validation, qualitative validation addresses the model behaviour in a more phenomenal way. Two aspects are highlighted; first the PCM heat of fusion changes, second the temperature of the surroundings varies. In both cases the response of the pouch will verify if the model behaves conform expectations.

The heat of fusion is a measure for the amount of energy that the PCM pouch accumulates during phase change. Increasing heat of fusion values account for larger amounts of accumulated energy, hence moderated temperature levels. Opposite, decreasing heats of fusion yield increasing temperature levels during phase change. While changing the PCM heat of fusion, all other properties remain as applied at the quantitative analysis. Graphs below show the results for 440 [kJ/kg] and 27.5 [kJ/kg] respectively.

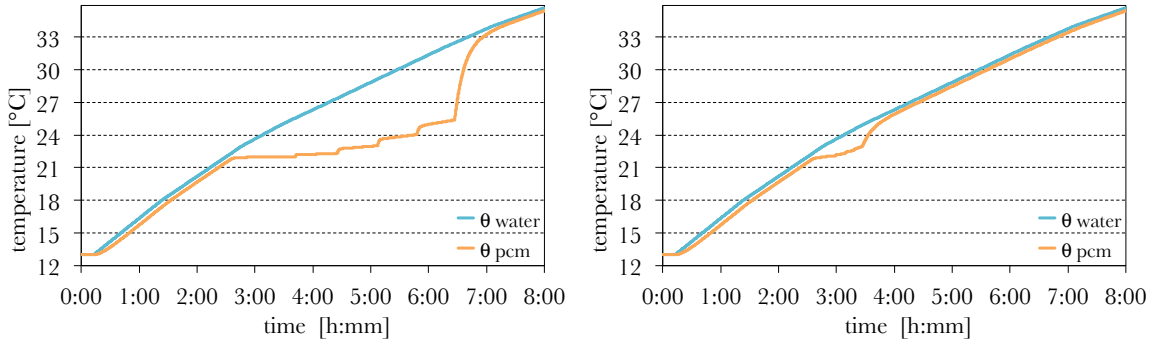

figure 5.5 *Pouch model validation by changing the PCM heat of fusion. A higher heat of fusion (440[kJ/kg] yields an increase in response delay (left) whereas a lower heat of fusion (27.5[kJ/kg] results in a faster response to the imposed water temperature (right).*

The surrounding temperature implies a certain energy exchange with the PCM pouch. A higher temperature gives rise to the PCM pouch temperature. On the other hand, if the surrounding temperature drops, the pouch temperature follows likewise. Supposedly the PCM temperature is delayed because of energy accumulation and energy transfer rates at the pouch surface. Indeed figures show such pouch performance (figure 5.6).

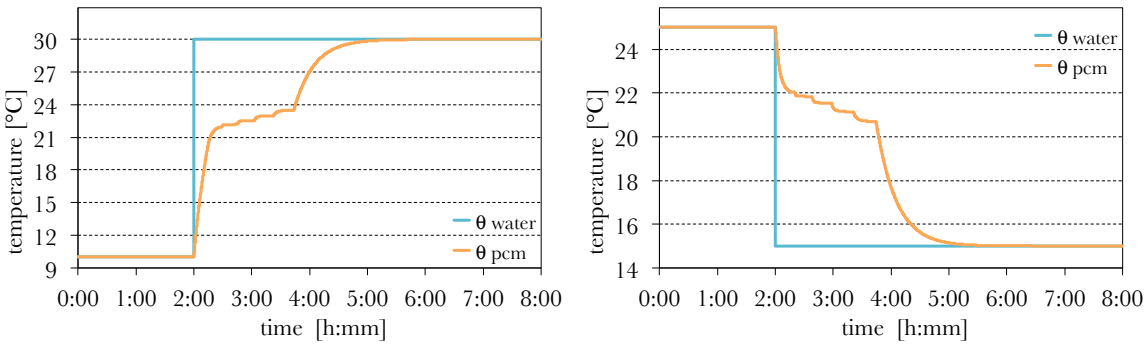

figure 5.6 *Pouch model validation by imposing surrounding temperature as step function. A temperature rise causes the pouch temperature to increase (left) while a temperature drop yields a pouch temperature decrease (right). PCM pouch reactions are delayed since it accumulates energy and because of energy exchange effects.*

5.4.3 Discussion

Ten layers of equal thickness compile the PCM pouch model, where surrounding air serves as heat transfer medium, resulting in a model that is symmetrical with respect to the two inmost layers, as the five steps in the diagrams bear out. The depicted pouch temperature equals the average temperature over all ten layers. Because the water bath experiments samples two pouches tied together with a thermocouple in between, a better comparison with the modelled pouch would have been obtained when the model consisted of two layers instead of ten.

The pouch division into ten layers indirectly justifies the lumped model approach. A uniform temperature distribution is reasonable to assume when the Biot number is much smaller than unity [33]. The error introduced is small, especially if the following condition satisfies:

$$\mathrm{Bi} = \frac{\alpha_C L}{\lambda} < 0.1 \qquad (5.9)$$

Where the characteristic length is defined as volume over surface area. For maximum pouch dimensions (1000 x 450 x 25 [mm]) at 'worst case' heat convection and conduction

coefficients, the Biot number is about 0.23, which is more than 0.1, but still much smaller than unity. Hence the uniform temperature assumption is justified.

Although the PCM pouch model behaves like real pouches, the graphs in figure 5.4 are not identical. Main difference is the gap between water temperature and PCM pouch temperature. As published by Climator, the manufacturer of C22 PCM [8], the heat of fusion of C22 is 110 [kJ/kg]. However, if the heat of fusion of the pouch model is set to a significant lower value, the pouch model temperature will show greater similarity to the measured temperature course.

6 RESULTS AND DISCUSSION

Prior to the issue of results, the Capacity Cube and PCM pouch models are assembled. In accordance with the Capacity Cube model setup, the PCM pouch model substitutes the single node that represents the pouch. Results (6.1) are compiled for four different kinds of PCMs, further the results are considered in the discussion section (6.2).

6.1 Results

Four types of PCMs are investigated (table 6.1). All of the pouches contain PCMs applicable to built environment, i.e. their phase change temperatures vary roughly between 22 [°C] to 25 [°C]. The sample PCMs are selected to point the differences in energy storage over nearly equal phase change temperatures.

Table 6.1 *PCM properties of the sample pouches that are used in the simulations (data provided by manufacturers [8, 49, 54, 62]).*

PCM	T_{pc} [°C]	ρ [kg/m^3]	c_p [J/kgK]	h_{lat} [kJ/kg]
SavENRG PCM22P	22	1690 *)	3056	185
PureTemp PT23	23	830	1915	203
ClimSel C24	24	1480	3600	144
PCM Energy P.Latest 25T	25	1490	2000	175

*) Specific mass varies over phases - the average value is 1690 [kg/m^3]

Simulations are carried out at 20 [°C] environmental temperature and with 0.25 [m/s] internal air speed. Pouch dimensions are 1000 [mm] long by 450 [mm] wide. The pouch thickness is 25 [mm]. Any of the PCMs is subjected to a complete thermal cycle from fully solid to fully liquid and back. Besides the pouches are also subjected to an incomplete cycle, from fully solid to half molten and back (figure 6.1 to figure 6.4). The specific reference enthalpy equals h(0) = 0 [kJ/kg].

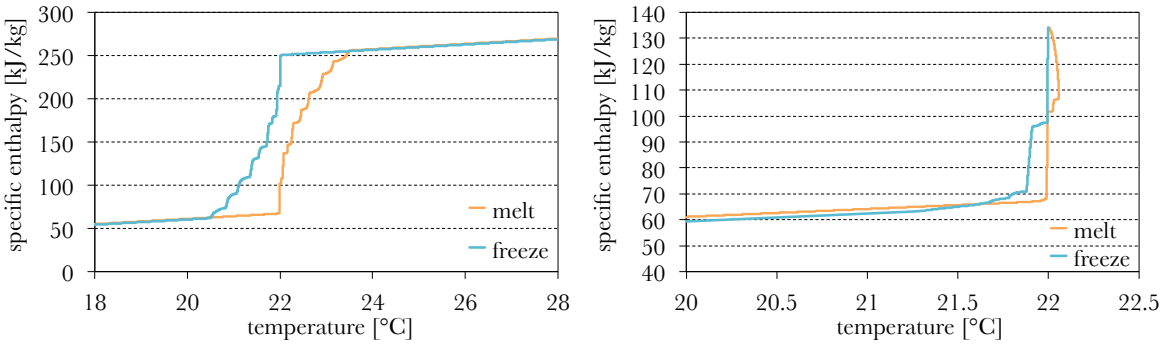

figure 6.1 *Simulation results for "SavENRG PCM22P" [54]; a full thermal cycle is shown left, a half thermal cycle is shown right. The full cycle graph is obtained with heating and cooling rates of 1.0 [K/h]. The half thermal cycle graph is obtained with an heating rate of 1.1 [K/h] and a cooling rate of 2.2 [K/h].*

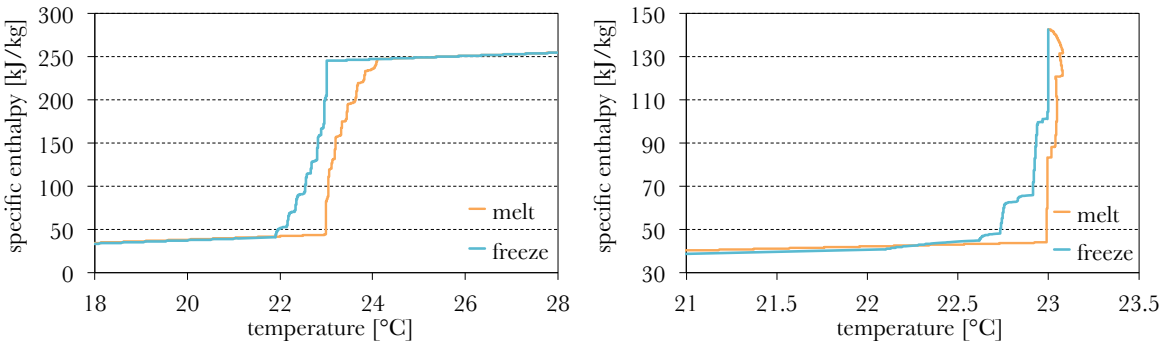

figure 6.2 *Simulation results for "PureTemp PT23" [49]; a full thermal cycle is shown left, a half thermal cycle is shown right. The full cycle graph is obtained with heating and cooling rates of 1.0 [K/h]. The half thermal cycle graph is obtained with an heating rate of 1.0 [K/h] and a cooling rate of 1.9 [K/h].*

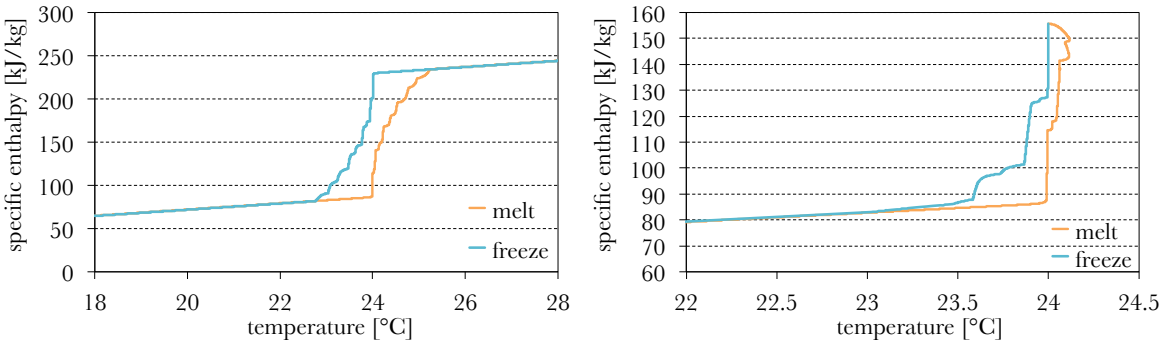

figure 6.3 *Simulation results for "ClimSel C24" [8]; a full thermal cycle is shown left, a half thermal cycle is shown right. The full cycle graph is obtained with heating and cooling rates of 1.0 [K/h]. The half thermal cycle graph is obtained with an heating rate of 1.0 [K/h] and a cooling rate of 3.6 [K/h].*

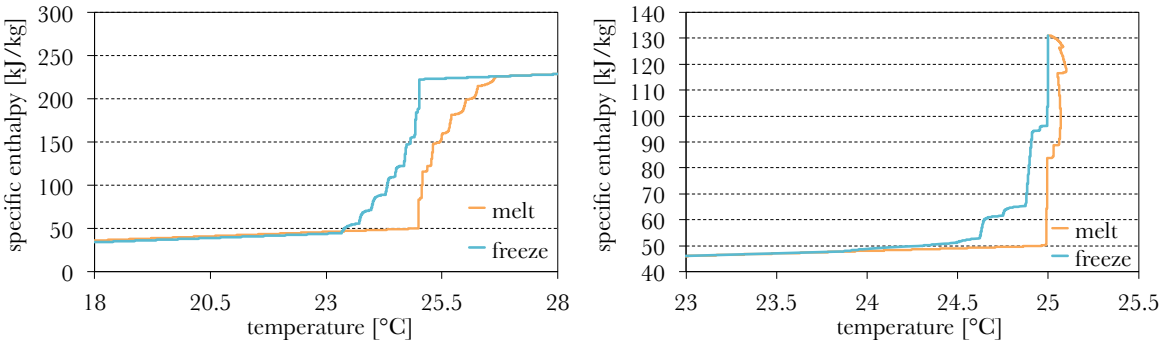

figure 6.4 *Simulation results for "PCM Energy P.Latest 25T" [62]; a full thermal cycle is shown left, a half thermal cycle is shown right. The full cycle graph is obtained with heating and cooling rates of 1.0 [K/h]. The half thermal cycle graph is obtained with an heating rate of 1.5 [K/h] and a cooling rate of 2.6 [K/h].*

The differences between heat flow input and heat losses from the Capacity Cube to the environment yield the amount of energy accumulation in the pouch or the energy transferred from the pouch (Table 6.2). Heat flows from the inner envelope walls to the center envelope walls quantify the heat losses. The input heat flow is derived from the mass flow and temperature difference over the nodes in the bottom air layer of the model, as given by:

$$Q_F = f\, c_p\, \Delta T \qquad (6.1)$$

Table 6.2 *Energy accumulation by the PCM pouches during phase change. Values are 24 [h] average.*

PCM	full cycle		half cycle	
	[kJ]	[kJ/kg]	[kJ]	[kJ/kg]
SavENRG PCM22P	233	12.3	115	6.1
PureTemp PT23	241	25.8	129	13.8
ClimSel C24	205	12.3	99	6.0
PCM Energy P.Latest 25T	234	14.0	120	7.2

6.2 Discussion

Results are analyzed by consideration of three aspects. A general interpretation of the outcome is given first (6.2.1). Further the relation to built environment is addressed (6.2.2). A comparison to similar methods (6.2.3) closes this section.

6.2.1 General interpretation

Melting and freezing curves coincide outside the phase change region only, when enthalpy is linearly related to temperature. During phase change the curves bend towards each other, almost touching in the middle, while the gap between the lines grows where phase change initiates or runs out. The slope is steepest at the very start of phase transition. Moreover the stepwise curve shows clearly.

The pouch model setup determines the graph shapes to great extent. Since the model consists of ten layers, graphs show the full pouch behaviour, averaged over all ten layers. Phase transition starts at the single bottom layer, progressing through the pouch until all layers have completed phase change. This also explains the sudden change from almost horizontal to nearly vertical related h(T) lines at the beginning of the phase change region; one layer changes phase first so that the enthalpy increases to heat of fusion values, while the other layers still exhibit purely liquid or solid state. Further the second layer and later the third and higher layers reach their phase transition temperatures, giving steps to the enthalpy curve. As the top layers change phase, the bottom layers are fully molten or solidified already, causing the enthalpy curve to increase less as a function of temperature, so that the curve bends to a more horizontal orientation as the full pouch phase change draws to an end.

Both melting and freezing curves start exactly at the phase change temprature, which is a model input and defined within the relatively small temperature range $T_{pc} \pm 0.01$ [K]. Melting and solidification lines reach each other closest in the middle, almost touching on the imaginary vertical line representing the phase change temperature. It is there the curves bend towards each other, because that point characterizes the state on both lines where approximately half of the pouch has changed phase.

6.2.2 Built environment relation

Built environment applications benefit most from PCMs that undergo full thermal cycles, because maximum amounts of energy are stored as the pouch fully changes from solid to liquid. Simulation results show that half cycles approximately store half the amount of energy of a full cycle, but correlations do not seem to be linearly related. The enthalpy temperature diagrams depict at the start of phase change a steep curve that flattens out as the phase change progresses through the pouch, which implies relatively higher energy storage during the initial stage of phase change. Furthermore inhomogeneous behaviour of the PCM pouches appears from the model simulations, in particular from the gap between melting and freezing curves. Hence, phase change does not occur at a single temperature, but takes place over a temperature range, which affects the PCM selection for use in built environment. Moreover the accumulated energy within pouches may differ significantly,

up to 12 [kJ/kg] for the regarded PCMs, even if the phase change temperatures differ merely a single degree in temperature.

6.2.3 Resemblance to comparable methods

Macroscopic PCM models have been reported by e.g. Egolf and Manz [17], and Feustel [21]. However the computational scheme proposed by Van Dorp [12] (figure 6.5) as well as the simulation model by Bony and Citherlet [4] gain outputs similar to the layered pouch model, especially with respect to the inhomogeneous behaviour, or 'hysteresis' as referred to by Van Dorp and Bony and Citherlet.

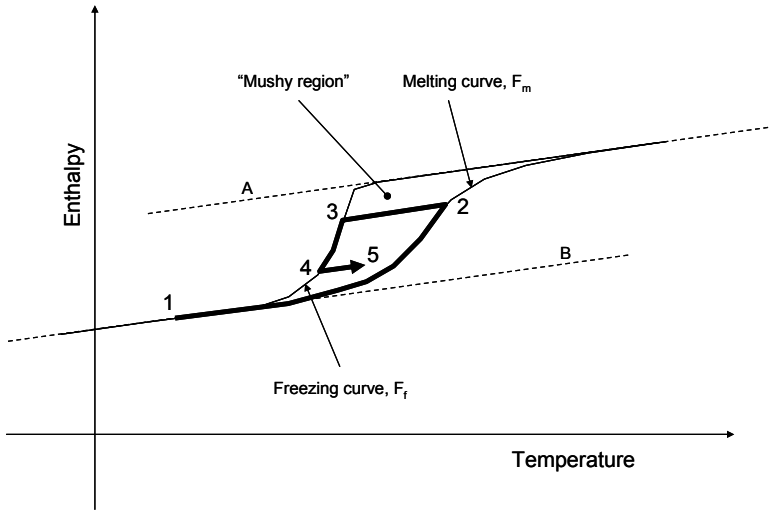

figure 6.5 *Enthalpy-temperature graph, sketch by Van Dorp to support the computational scheme [12]. Bony and Citherlet [4] presented a similar diagram.*

Graphs obtained with the layered pouch model are similar to the graph in the figure above. Freezing and melting curves do not coincide, unless pure liquid or solid state is concerned. Both methods exhibit steep curve slopes at the start of phase change. But an important difference is shown for incomplete thermal cycles; the departure from point 2 (figure 6.5) runs parallel to line A (figure 6.5) which represents the specific heat in liquid state. However, if departure from the same point is supposed, the layered PCM pouch model yields a line parallel to the freezing curve. Hence further research is required.

7 CONCLUSIONS AND RECOMMENDATIONS

7.1 Conclusions

Phase Change Materials (PCMs) store or release energy by changing phase from solid to liquid or vice versa. Successive melting and freezing transitions are referred to as thermal cycling. Incomplete thermal cycling affects the storage capacity of PCMs. This work focuses on the latter drawback of PCM applications: What is the impact of incomplete thermal cycling on the energy storage capacity of PCM pouches as applied in built environment?

Existing measuring techniques lack the ability to test bulk material PCMs within air surroundings. Therefore the Capacity Cube is newly designed and modelled to perform simulations with. The Capacity Cube is a measuring device that puts live size PCM pouches to the test, while it uses surrounding air as heat transferring medium. The heat source is a thermo-electrical module, whereas an axial fan enforces the heated air to flow around the pouch. Temperature transmitters and electrical power input provide the required information to control the Capacity Cube inside temperatures that are the driving force for heat transfer.

A general model of a PCM pouch is compiled to use with the Capacity Cube model. The pouch model consists of ten layers of equal thickness. Simulation outputs are enthalpy-temperature graphs. These graphs clearly show that PCM 'hysteresis' as it is sometimes referred to, appears to be inhomogeneous behaviour of the material. Melting and freezing curves coincide for pure, single phases only, because during phase transition part of the PCM has already changed phase when another part of the PCM holds its initial state still. It is this inhomogeneous behaviour that also explains the sudden enthalpy increase at the start of phase change. As phase change for the full pouch finalizes the enthalpy curve loses its steepness and flattens out towards the straight line representing the specific heat.

Defective thermal cycling does affect the storage capacity significantly. For half cycles the storage capacity halves likewise. Regarding the steepness of the enthalpy-temperature curves, it is expected half cycles correspond with more than half of the energy accumulation, however this is not supported by simulation results.

7.2 Recommendations

Although the presented models provide useful information, real time measurements are not carried out with the Capacity Cube. Real time measurements help to improve the model and match it with live results. Therefore the Capacity Cube should be developed and a prototype should be build to perform experiments with.

To predict the impact of thermal cycling in the very long run, the model needs to be augmented with aging aspects. After repeated cycles the PCMs behaviour is expected to alter because of changes in its crystal structure, fouling or other aging effects.

The PCM pouch model shows similarities to numerical methods presented by Van Dorp [12] and Bony and Citherlet [4], however within the phase change region the pouch model deviates from these methods. Hence, model improvement is required. Contrary to the present numerical, macroscopic models, it is proposed to improve the PCM model with the enthalpy relation that is given by the mean value of freezing curve and melting curve within the phase change region, instead of the average between 'A' and 'B' (figure 7.1). Such an enthalpy-temperature relation suits the 'half liquid, half solid' character of the mushy region. Moreover it is midway between the numerical models and simulation results of the layered pouch model.

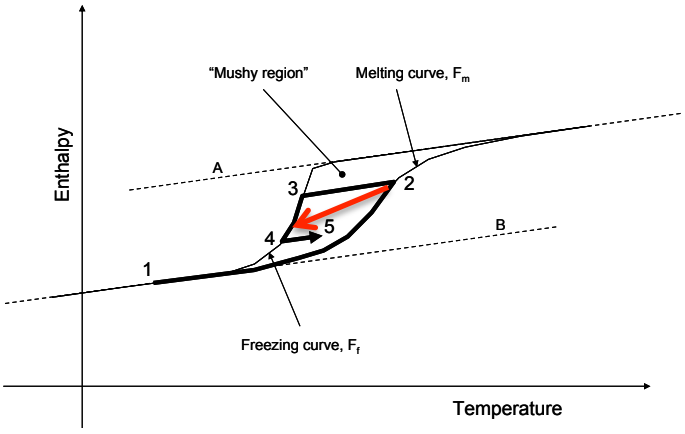

figure 7.1 *Proposed model improvement within the phase change region. Such an enthalpy-temperature relation suits the mushy region characteristics.*

ACKNOWLEDGEMENTS

I am immensely indebted to Carlos Infante Ferreira who advised me thoughtfully, criticized my work in detail and encouraged me kindly while compiling this work. I am especially thankful to Carlos for his patience.

Appreciation is extended to Joris van Dorp for his support and valuable input. Laure Itard is acknowledged for helping me through the subject of Indoor Climate Design.

I am forever grateful to wonderful Wina, for her love, support and perpetual patience.

Sander Koekenbier
Amsterdam, September 2011

REFERENCES

[1] Abhat, A.
Low temperature latent heat thermal energy storage: heat storage materials
Solar Energy 30, no.4 (1983) 313-332

[2] Arkar, C.; Vidrih, B.; Medved, S.
Efficiency of free cooling using latent heat storage integrated into the ventilation system of a low energy building
International Journal of Refrigeration 30 (2007) 134-143

[3] Bach, P.W.; Haije, W.G.
Heat storage and transformation
presented at ZAE symposium, Germany, 2001
available online: http://www.ecn.nl/docs/library/report/2001/rx01036.pdf

[4] Bony, J.; Citherlet, S.
Simulation model of PCM modules plunged in a water tank (type 860)
Contribution to "Simulation models of PCM storage units – a report of IEA solar heating and cooling programme, task 32; advanced storage concepts for solar and low energy buildings"
Task 32 Storage / IEA, Report C5 of subtask C, 2008

[5] Bosgra, O.H.
Inleiding modelvorming, lecture notes WB2311, TU Delft - TU/e
Delft University of Technology, Delft, Netherlands, 2004

[6] Bouwman, I.M.
Passive cooling: feasible or not? Feasibility of passive cooled lightweight buildings based on heat accumulation in PCM
Delft University of Technology / HunterDouglas, Delft, Netherlands, 2006

[7] Churchill, S.W.; Chu, H.H.S.
Correlating equations for laminar and turbulent free convection from a vertical plate
International Journal of Heat and Mass Transfer 18 (1975) 1323-1329

[8] Climator, ClimSel datasheets, available online:
http://www.climator.com/en/climsel/

[9] Darkwa, K.
Evaluation of regenerative phase change drywalls: low-energy buildings application
International Journal of Energy Research 23 (1999) 1205-1212

[10] Dinçer, I.; Rosen, M.A.
Thermal energy storage – systems and applications
John Wiley & Sons, New York, United States of America, 2002
[11] Dodd, J.W.; Tonge, K.H.
Thermal methods
John Wiley & Sons, London, England, 1987
[12] Van Dorp, J.E.
A computational scheme for approximating phase change material behaviour
To be published
[13] Van Dorp, J.E.
An approach to empirical investigation of performance of passive PCM applications in office buildings based on the T-history method
Arcadis, Den Haag, Netherlands, 2004
[14] Le Dréau, J.; Karlsen, L.; Litewnicki, M.; Michaelsen, L.; Møllerskov, A.; Ødegaard, H.; Svendsen, L.; Jensen, R.L.; Marszal, A.
Experimental investigation of the influence of different flooring emissivity on night-time cooling using displacement ventilation
presented at the 9th Nordic Symposium on Building Physics 2011
available online: http://vbn.aau.dk/files/52824156/Experimental_Investigation...
... _of_the_Influence_of_Different_Flooring_Emissivity_on_Night_Time_Cooling...
... _using_Displacement_Ventilation.pdf
[15] Ebm-Papst fans, website: www.ebmpapst.com
[16] Ebm-Papst axial fans product catalogue 2011, available online:
http://www.ebmpapst.com/en/products/axial-fans/axial_fans.php
[17] Egolf, P.W.; Manz, H.
Theory and modeling of phase change materials with and without mushy regions
International Journal of Heat and Mass Transfer 37, no.18 (1994) 2917-2924
[18] Energy research Centre of the Netherlands (ECN)
ECN description of Differential Scanning Calorimetry
Available online: http://www.ecn.nl/serviceloket/meten-testen/...
.../fysische-karakterisering/differential-scanning-calorimetry/publicatie
[19] Farid, M.; Kong, W.J.
Underfloor heating with latent heat storage
Proceedings Institution of Mechanical Engineers 215, part A (2001) 601-609
[20] Farid, M.M.; Chen, X.D.
Domestic electrical space heating with heat storage
Proceedings Institution of Mechanical Engineers 213, part A (1999) 83-92
[21] Feustel, H.E.
Simplified numerical description of latent storage characteristics for phase change wallboard
University of California, Berkeley, United States of America, 1995

[22] Goldstein, R.J.; Sparrow, E.M.; Jones, D.C.
Natural convection mass transfer adjacent to horizontal plates
International Journal of Heat and Mass Transfer 16 (1973) 1025-1035

[23] Golomb, S.W.
Mathematical models: uses and limitations
IEEE transactions on reliability 20, no.3 (1971) 130-131

[24] Gong, Z-X.; Mujumdar, A.S.
Enhancement of energy charge-discharge rates in composite slabs of different phase change materials
International Journal of Heat and Mass Transfer 39, no.4 (1996) 725-733

[25] Grolier, J-P. E.; Dan, F.; Boyer, S.; Orlowska, M.; Randzio, S.L.
The use of scanning transitiometry to investigate thermodynamic properties of polymeric systems over extended T and p ranges
International Journal of Thermophysics 25, no.2 (2004) 297-319

[26] Günther, E.; Hiebler, S.; Mehling, H.
Determination of the heat storage capacity of PCM and PCM-objects as a function of temperature
presented at 10th International Conference on Thermal Energy Storage, USA, 2006
available online: http://intraweb.stockton.edu/eyos/energy_studies/content/…
…/docs/FINAL_PAPERS/11B-2.pdf

[27] Hasnain, S.M.
Review on sustainable thermal energy storage technologies, part 1: heat storage materials and techniques
Energy Conversion Management 39, no.11 (1998) 1127-1138

[28] Hauer, A.; Mehling, H.; Schossig, P.; Yamaha, M.; Cabeza, L.; Martin, V.; Setterwall, F.
IEA implementing agreement on energy conservation through energy storage
annex 17 final report
International Energy Agency, Canada, 2001

[29] Himran, S.; Suwono, A.; Mansoori, G.A.
Characterization of alkanes and paraffin waxes for application as phase change energy storage medium
Energy Sources 16 (1994) 117-128

[30] Hong, H.; Kim, S.K.; Kim, Y-S.
Accuracy improvement of T-history method for measuring heat of fusion of various materials
International Journal of Refrigeration 27 (2004) 360-366

[31] Howell, J.R.
A catalog of radiation heat transfer configuration factors
McGraw-Hill, New York, United States of America, 1982
3rd edition available online: http://www.engr.uky.edu/rtl/Catalog/

[32] Ibáñez, M.; Lázaro, A.; Zalba, B.; Cabeza, L.F.
An approach to the simulation of PCMs in building applications using TRNSYS
Applied Thermal Engineering 25 (2005) 1796-1807
[33] Incropera, F.P.; DeWitt, D.P.; Bergman, T.L.; Lavine, A.S.
Fundamentals of heat and mass transfer, 6th edition
John Wiley & Sons, Hoboken, United States of America, 2007
[34] Infrared Services
Emissivity values for common materials, tables available online:
http://www.infrared-thermography.com/material.htm
[35] Jakob, M.
Heat transfer, volume I
John Wiley & Sons, New York, United States of America, 1949
[36] Kaletunç, G. (editor)
Calorimetry in food processing: analysis and design of food systems
Wiley-Blackwell, Ames, United States of America, 2009
[37] Kimura, H.; Kai, J.
Mixtures of calcium chloride hexahydrate with salt hydrate or anhydrous salts as latent heat storage materials
Energy Conversion Management 28, no.3 (1988) 197-200
[38] Koekenbier, S.F.
Introduction to phase change materials. Literature review, theoretical backgrounds, applications and sustainability aspects of PCMs as applied in built environment.
Delft University of Technology, Delft, Netherlands, 2009
[39] Koschenz, M.; Lehmann, B.
Development of a thermally activated ceiling panel with PCM for application in lightweight and retrofitted buildings
Energy and Buildings 36 (2004) 567-578
[40] Van den Kroonenberg, H.H.; Siers, F.J.
Methodisch ontwerpen. Ontwerpmethoden, voorbeelden, cases, oefeningen.
Educatieve Partners Nederland, Houten, Netherlands, 1998
[41] Kwatny, H.G.; Mablekos, V.E.
The modelling of dynamical processes
Proceedings of the 1975 IEEE conference on decision and control (1975) 271-281
[42] Lane, G.A.
Solar heat storage: latent heat materials - volume 1: background and scientific principles
CRC press, Boca Raton, United States of America, 1983
[43] Leijendeckers, P.H.H.; Fortuin, J.B.; Van Herwijnen, F.; Schwippert, G.A. (editors)
Polytechnisch Zakboek, 49e druk
Elsevier Bedrijfsinformatie, Arnhem, Netherlands, 2002

[44] Marín, J.M.; Zalba, B.; Cabeza, L.F.; Mehling, H.
Determination of enthalpy-temperature curves of phase change materials with the temperature-history method: improvement to temperature dependent properties
Measurement Science and Technology 14 (2003) 184-189

[45] McNichols perforated products, datasheets, available online:
http://www.mcnichols.com/products/perforated/round-hole/

[46] Mehling, H.; Ebert, H-P.; Schossig, P.
Development of standards for materials testing and quality control of PCM
presented at 7th II Conference on Phase Change Materials and Slurries for Refrigeration and Air Conditioning, France, 2006
available online: http://www.pcm-ral.de/pdf/Paperfinal.pdf

[47] Orlowska, M.; Randzio, S.L.
Simultaneous and in situ analysis of thermal and volumetric properties of starch gelatinization over wide pressure and temperature ranges
Biomacromolecules 6 (2005) 3045-3050

[48] Van Paassen, A.H.C.; Van Dorp, J.E.
Centrale luchtbehandeling met behulp van PCM
RCC Koude & Luchtbehandeling B, nr.3 (2008) 15-19

[49] PureTemp PCM products, PCM PT23 datasheet available online:
http://www.puretemp.com/technology.html

[50] RAL Gutegemeinschaft
Quality and testing regulations for phase change materials - PCM
http://www.pcm-ral.de/en/ral-quality.htm

[51] Randzio, S.L.
Scanning transitiometry for science and industry
Journal of Thermal Analysis 48 (1997) 573-583

[52] Randzio, S.L.
State variables in calorimetric investigations: experimental results and their theoretical impact
Thermochimica Acta 300 (1997) 29-41

[53] Randzio, S.L.; Stachowiak, Ch.; Grolier, J-P. E.
Transitiometric determination of the three-phase curve in asymmetric binary systems
Journal of Chemical Thermodynamics 35 (2003) 639-648

[54] RGees PCM products, PCM22P datasheet available online:
http://www.rgees.com/product_PCM22P.php

[55] Rucon fans, website: www.rucon.nl

[56] Rydstrand, M.; He, B.; Martin, V.; Setterwall, F.
First experiments on Climsel 7 - a phase change material for cool thermal storage
presented at 6th Annex 17 Workshop, Sweden, 2004
available online: http://www.fskab.com/Annex17/Workshops/EM6%20Arvika/...
...Presentations/Rydstrand%20et%20al%20Paper%20First%20experiments...
...%20on%20climsel%207.pdf

[57] Sari, A.
Eutectic mixtures of some fatty acids for low temperature solar heating applications: thermal properties and thermal reliability
Applied Thermal Engineering 25 (2005) 2100-2107
[58] Sharma, A.; Sharma, S.D. Sharma; Buddhi, D.
Accelerated thermal cycle test of acetamide, stearic acid and paraffin wax for solar thermal latent heat storage applications
International Journal of Energy Conversion and Management 43, no.14 (2002) 1923-1930
[59] Shukla, A.; Buddhi, D.; Sharma, S.D.; Sagara, K.
Accelerated thermal cycle test of erythritol for the latent heat storage application presented at 4th Annex 17 workshop, India 2003
available online: http://www.fskab.com/Annex17/Workshops/…
…/EM4%20Indore%202003-03-21--24/Presentations/paper_annat.pdf
[60] Sparrow, E.M.; Carranco Ortiz, M.
Heat transfer coefficients for the upstream face of a perforated plate positioned normal to an oncoming flow
International Journal of Heat and Mass Transfer 25, no.1 (1982) 127-135
[61] Stritih, U.; Butala V.
Energy saving in building with PCM cold storage
International Journal of Energy Research 31, no.15 (2007) 1532-1544
[62] Teap PCM products, P.Latest 25T datasheet available online:
http://www.teappcm.com/products.htm
[63] Tetech air-cooler products specification
available online: http://www.tetech.com/docs/AC-162.pdf
[64] Tetech, email conversation Paul Lau, Engineering/Sales division, march/april 2011
[65] Ting, K.C.; Giannakakos, P.N.; Gilbert, S.G.
Durability of latent heat storage tube sheets
Solar Energy 39, no.2 (1987) 79-85
[66] Tombling fans, website: www.tombling.com
[67] Universal Construction Foam, EPS datasheet, available online:
http://www.universalconstructionfoam.com/downloads/eps-data-sheet.pdf
[68] Weston Isolatie, EPS datasheet, available online:
http://www.weston.nl/sites/weston.nl/files/Technische_20gegevens_20EPS.pdf
[69] Willems, J.C.
Paradigms and puzzles in the theory of dynamical systems
IEEE transactions on automatic control 36, no.3 (1991) 259-294
[70] Zalba, B.; Marín, J.M.; Cabeza, L.F.; Mehling, H.
Review on thermal energy storage with phase change: materials, heat transfer analysis and applications
Applied Thermal Engineering 23 (2003) 251-283

[71] Zhang, Y.; Jiang, Y.; Jiang, Y.
A simple method, the T-history method, of determining the heat of fusion, specific heat and thermal conductivity of phase change materials
Measurement Science and Technology 10 (1999) 201-205

[72] Zivkovic B.; Fujii I.
An analysis of isothermal phase change of phase change material within rectangular and cylindrical containers
Solar Energy 70, no.1 (2001) 51-61

[73] Zwicky, F.
Morphological Astronomy
The Observatory 68, no.845 (1948) 121-143

[74] Zwicky, F.
The Morphological Method of Analysis and Construction
Courant, Intersciences Publishers, Anniversary Volume (1948) 461-470

APPENDICES

The Appendices focus on the three modes of heat transfer and the corresponding heat transfer coefficients as used in the models of the Capacity Cube and the PCM pouch (figure A.1). Air is forced to flow from bottom to top along the PCM pouch and along the inner walls of the Capacity Cube. Convective heat transfer is present at both the inside and outside of the Capacity Cube. Moreover heat conduction within solid material layers occurs besides radiation between mutual walls and radiation between walls and PCM pouch. The four regions A, B, C, and D make it easier to discern differences in the heat transfer coefficients present in the particular region.

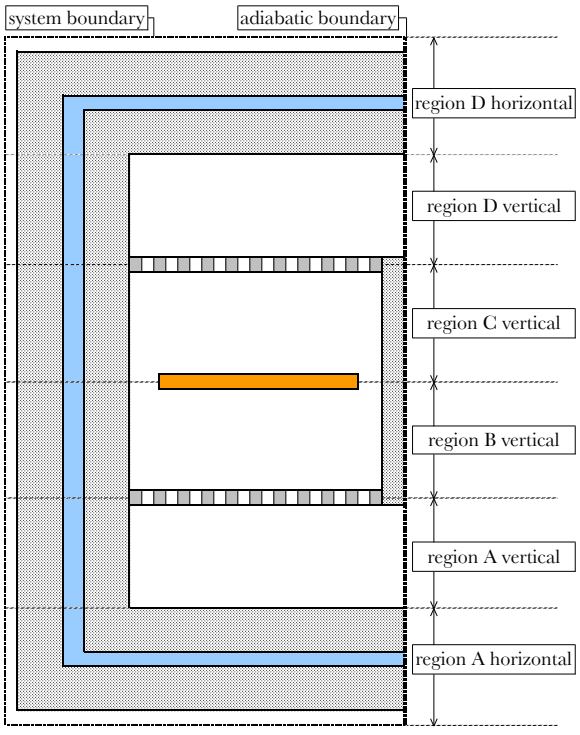

figure A.1 *Overview of the Capacity Cube that contains the PCM pouch. Convective heat transfer is present at the inner and outer walls and at the pouch, conductive heat transfer occurs within solid material layers and radiation takes place between solid materials that 'see' each other. Note the four distinguished regions A, B, C and D.*

Appendix A Heat conduction coefficients

The basic law of heat conduction is given by:

$$Q_D = \lambda \frac{A}{d} \Delta T \tag{A.1}$$

Rearranging yields:

$$Q_D = \frac{\lambda}{d} A \Delta T \tag{A.2}$$

Where the ratio λ/d is constant since both the thermal conductivity and the material thickness are time and temperature invariant. Therefore λ/d is substituted by the conductive heat transfer coefficient:

$$\alpha_D = \frac{\lambda}{d} \tag{A.3}$$

And the equation for heat conduction becomes:

$$Q_D = \alpha_D A \Delta T \tag{A.4}$$

Numerical values for the heat transfer coefficients of conduction as used in the models of the Capacity Cube and the PCM pouch are given in table A.1.

table A.1 *Heat transfer coefficients of conduction for the materials used in the model of the Capacity Cube and in the model of the PCM pouch. Values are provided by manufacturers [8, 45] and taken from literature [43].*

material	thickness	thermal conductivity	heat conduction coefficient
polystyreen	100 [mm]	0.08 [W/mK]	0.8 [W/m^{2}K]
glass	4 [mm]	0.93 [W/mK]	232.5 [W/m^{2}K]
polypropylene	1.6 [mm]	0.12 [W/mK]	75 [W/m^{2}K]
PCM minimum	25 [mm]	0.50 [W/mK]	20.0 [W/m^{2}K]
PCM maximum	10 [mm]	0.70 [W/mK]	70.0 [W/m^{2}K]

Appendix B Heat convection coefficients

The fundamental equation of heat convection is given by:

$$Q_C = \alpha_C A \Delta T \tag{A.5}$$

The heat convection coefficient can be derived from the Nusselt number:

$$\overline{Nu_L} \equiv \frac{\alpha_C L}{k} = f\left(Re_L, Gr_L, Pr\right) \tag{A.6}$$

Where the Reynolds, Grashof and Prandtl numbers are:

$$Re_L = \frac{\rho v_\infty L}{\mu} \tag{A.7}$$

$$Gr_L = \frac{g\beta\left(T_S - T_\infty\right)L^3}{\nu^2} \tag{A.8}$$

$$Pr = \frac{\nu}{\delta} \tag{A.9}$$

In case free or natural convection boundary layers are present, the Rayleigh number defines the ratio of buoyancy forces and thermal diffusivity according to the product of Grashof and Prandtl numbers:

$$Ra_L = Gr_L\, Pr = \frac{g\beta\left(T_S - T_\infty\right)L^3}{\nu\delta} \tag{A.10}$$

The characteristic length L usually represents the diameter of a circular surface or the length of a rectangular surface. However, in case flat plates are considered, the accuracy of correlations improves when the characteristic length is defined as the ratio of plate surface area over perimeter [22, 33]:

$$L = \frac{A}{P} \tag{A.11}$$

Correlations for the average Nusselt number largely depend on flow geometry, boundary layer conditions and free or forced convection effects. The Capacity Cube wall segments as well as the PCM pouch and the air guidance grids act either as vertical or horizontal flat plates, depending on the orientation of the segment of interest. Following configurations are distinguished when determining the average heat convection coefficients:

- cross flow around the horizontal PCM pouch
- parallel flow along the Capacity Cube inner walls
- transverse flow through the horizontal air guidance grids
- external flow along the Capacity Cube outer walls

In both situations of cross flow around the PCM pouch and parallel flow along the Capacity Cube inner walls the effects of free and forced convection are comparable, which is generally the case when $Gr/Re^2 \approx 1$. Forced convection effects may be omitted if $Gr/Re^2 \gg 1$ whereas free convection effects may be neglected when $Gr/Re^2 \ll 1$ [33, p.565].

B.1 Convection: cross flow around PCM pouch

For cross flow around the PCM pouch the correlation due to Hilpert [33, p.426] gives:

$$\overline{Nu_L} = 0.228\, Re_L^{0.731} \sqrt[3]{Pr} \qquad (A.12)$$

In case of forced convection over the PCM pouch, the heat convection coefficients vary only slightly with temperature in the boundary layer region (figure A.2).

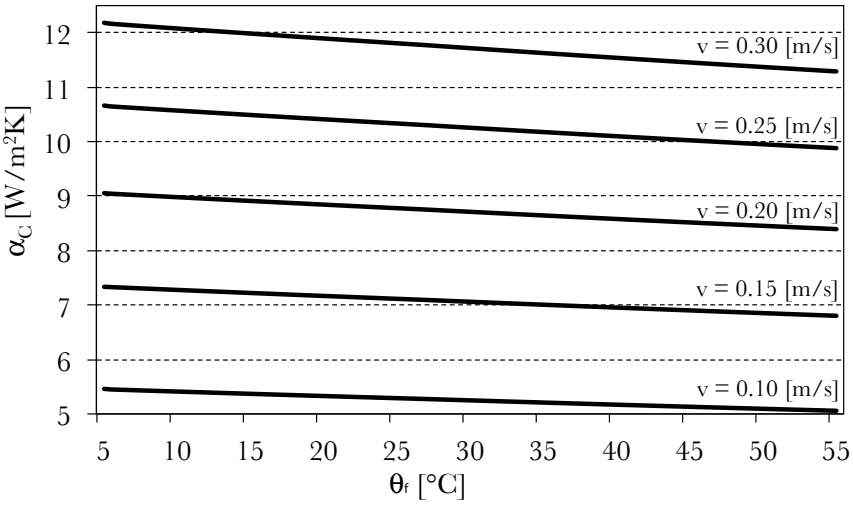

figure A.2 *Forced convection heat transfer coefficients as functions of the film temperature between PCM pouch and crossing airflow. At air velocities up to 0.30 [m/s] the forced heat convection coefficients are weak functions of temperature.*

Free convection effects cannot be disregarded since situations may occur for which $Gr/Re^2 \approx 1$, hence free convection and forced convection effects are comparable,

specifically when $T_{pouch} > T_{air}$. The Nusselt correlations for free convection separate the upper and lower surface of the pouch according to [33, p.577]:

$$\text{upper surface:} \quad \begin{cases} \overline{Nu_L} = 0.54\sqrt[4]{Ra_L} & \text{if} \quad 10^4 \le Ra_L \le 10^7 \\ \overline{Nu_L} = 0.15\sqrt[3]{Ra_L} & \text{if} \quad 10^7 < Ra_L \le 10^{11} \end{cases} \tag{A.13}$$

$$\text{lower surface:} \quad \overline{Nu_L} = 0.27\sqrt[4]{Ra_L} \quad \text{if} \quad 10^5 \le Ra_L \le 10^{10} \tag{A.14}$$

Free convection coefficients are weak functions of temperature. Higher temperature differences between pouch and surrounding airflow yield higher free convection coefficients. The graphs below show values for the heat transfer coefficient values when pouch and flow temperatures differ 0.5 [°C] (figure A.3) and 10 [°C] (figure A.4), with $T_{pouch} > T_{flow}$.

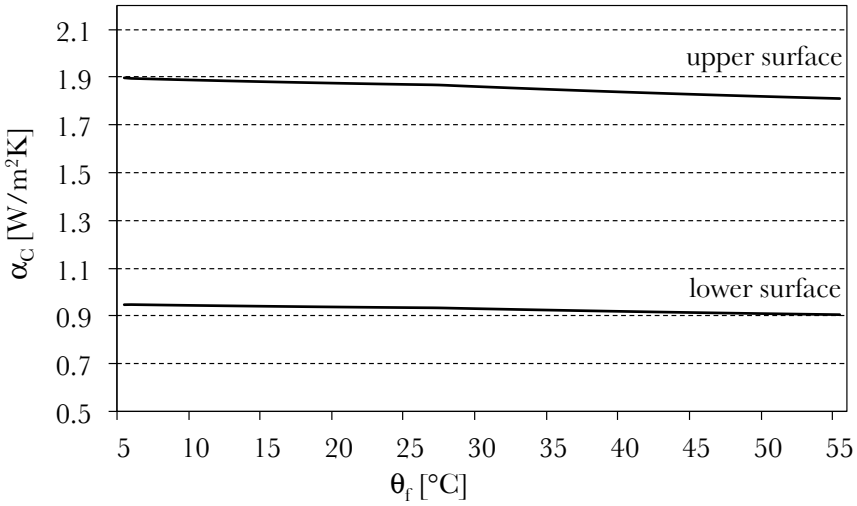

figure A.3 *Free convection heat transfer coefficients as functions of the film temperature between PCM pouch and crossing airflow. Free convection coefficients for upper and lower pouch surfaces are shown for $T_{pouch} - T_{flow} = 0.5$ [°C].*

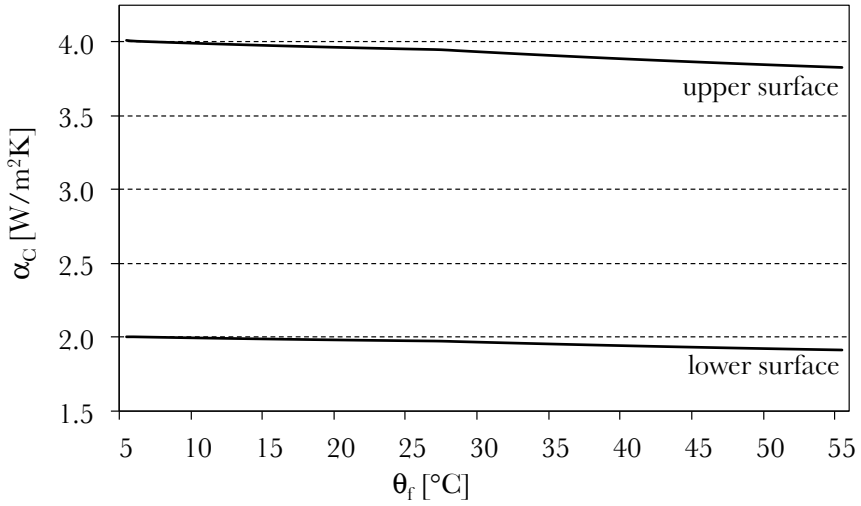

figure A.4 *Free convection heat transfer coefficients as functions of the film temperature between PCM pouch and crossing airflow. Free convection coefficients for upper and lower pouch surfaces are shown for $T_{pouch} - T_{flow} = 10$ [°C].*

In case of combined free and forced convection between the PCM pouch and transverse airflow the Nusselt correlation for mixed convection heat transfer is given by [33, p.594]:

$$\mathrm{Nu}_{\mathrm{mixed}}^{7/2} = \mathrm{Nu}_{\mathrm{forced}}^{7/2} + \mathrm{Nu}_{\mathrm{free}}^{7/2} \tag{A.15}$$

Both free and forced convection coefficients are weak functions of temperature. Accordingly the mixed convection coefficients are weak functions of temperature as well (figure A.5). Mixed convection transfer coefficients at the upper surface of the pouch are slightly higher than mixed transfer convection coefficients at the pouch lower surface.

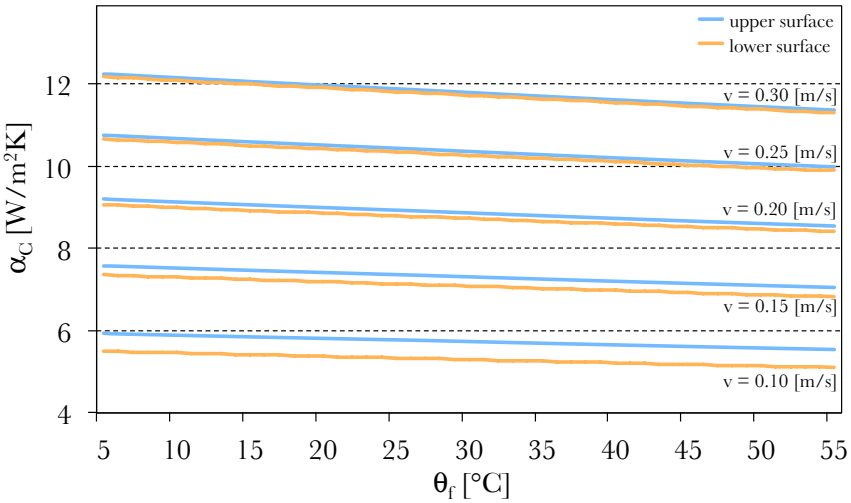

figure A.5 *Mixed convection heat transfer coefficients as functions of the film temperature between PCM pouch and crossing airflow. Mixed convection coefficients for upper and lower pouch surface are shown for $T_{pouch} - T_{flow} = 10$ [°C].*

B.2 Convection: parallel flow along CC inner walls

Forced airflow along the Capacity Cube inner walls determines the flow configuration for all wall segments as parallel flow over a flat plate. The corresponding Nusselt correlations yield [33, p.410/412]:

$$\overline{Nu_L} = 0.664\sqrt{Re_L}\sqrt[3]{Pr} \qquad \text{for laminar flow} \qquad (A.16)$$

$$\overline{Nu_L} = \left(0.037 Re_L^{0.8} - 871\right)\sqrt[3]{Pr} \qquad \text{for turbulent flow} \qquad (A.17)$$

Transition from laminar flow to turbulent flow in a forced convection boundary layer corresponds with $Re = 5 \cdot 10^5$ [33, p.361]. Transition from laminar to turbulent in a free convection boundary layer corresponds with $Ra \approx 10^9$ [33, p.569]. However, the boundary layer turns out to be laminar for all applicable flow configurations at air speeds having orders of magnitude from 10^{-1} to 10^0.

Conform the Capacity Cube geometry two unique vertical wall segments are distinguished; one 'long' (L = 1100 [mm]) segment and one 'short' (L = 550 [mm]) segment. Since the CC nodal model is a two dimensional model, the wall properties are simulated by a single node, so heat convection coefficients are averaged over the total wall surface:

$$\alpha_{average} = \frac{\sum A_i \alpha_i}{\sum A_i} \qquad (A.18)$$

Where index i denotes the particular wall segments of interest.

In case of forced convection along the horizontal inner walls of the Capacity Cube, the heat convection coefficients vary only slightly with temperature in the boundary layer region (figure A.6).

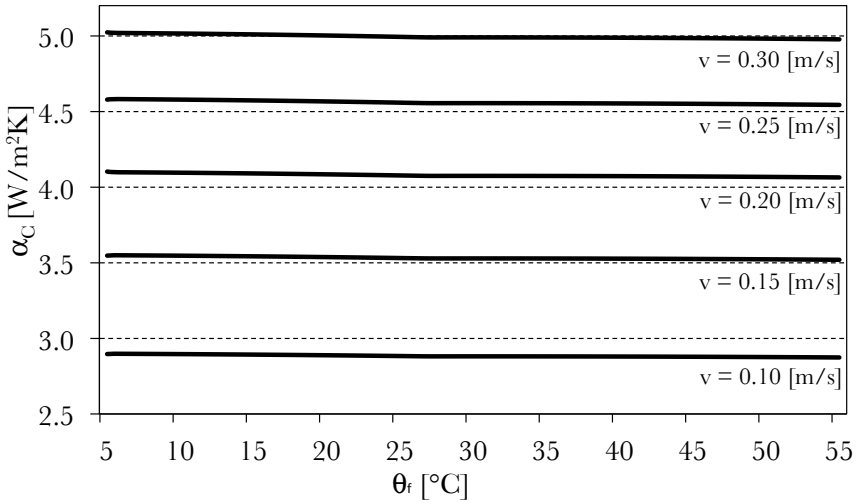

figure A.6 *Forced convection heat transfer coefficients as functions of the film temperature between the CC horizontal inner walls (regions A and D only) and parallel airflow. At air velocities up to 0.30 [m/s] the forced heat convection coefficients are weak functions of temperature.*

Also in case of forced convection along the CC vertical inner walls, the heat convection coefficients are nearly constant functions of the boundary layer temperature (figure A.7 and figure A.8).

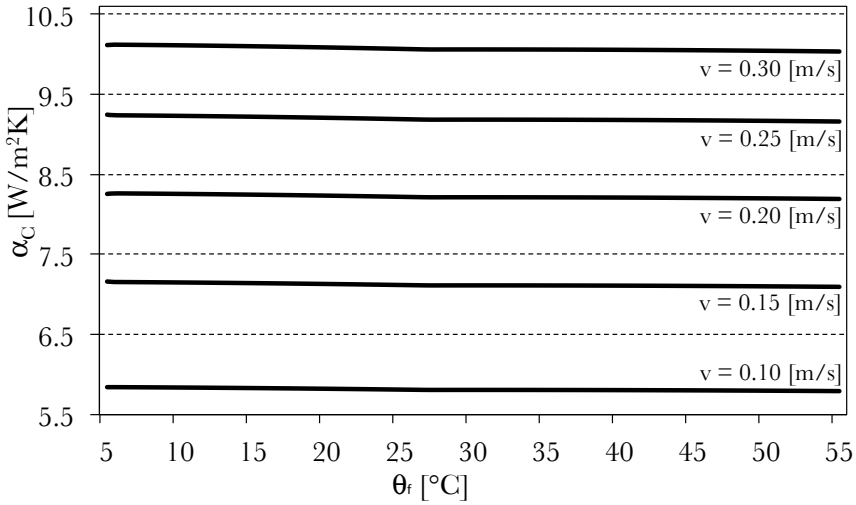

figure A.7 *Forced convection heat transfer coefficients as functions of the film temperature between the CC vertical inner walls in regions A and D and parallel airflow. The forced heat convection coefficients are nearly constant functions of temperature.*

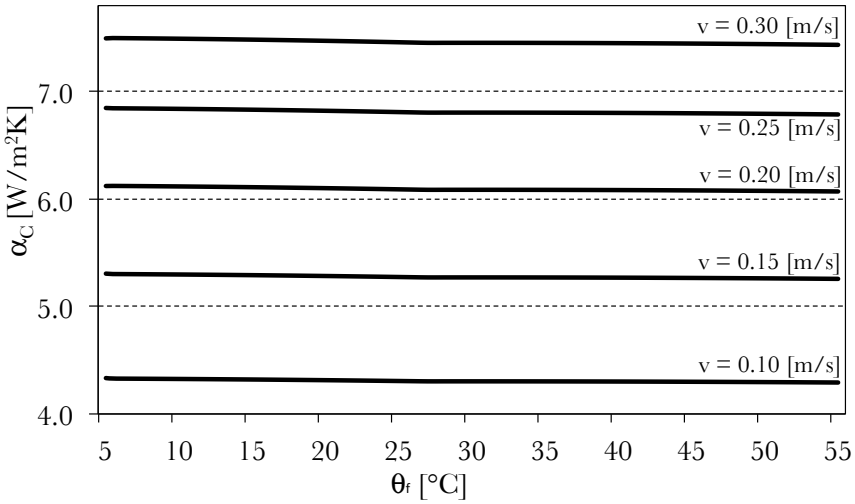

figure A.8 *Forced convection heat transfer coefficients as functions of the film temperature between the CC vertical inner walls in regions B and C and parallel airflow. The forced heat convection coefficients are nearly constant functions of temperature.*

Like free convection along the PCM pouch, free convection along the inner walls only plays a role if the temperature of the wall surpasses the flow temperature. In case the wall temperature is lower than the flow temperature, the criterion $Gr / Re^2 \ll 1$ is satisfied and free convection effects may be neglected.

When the horizontal walls in regions A and D are considered, the free convection correlations for upper and lower surfaces of hot or cold plates give [33, p.577]:

Upper surface of horizontal wall A:

$$\overline{Nu_L} = 0.54\sqrt[4]{Ra_L} \quad \text{if} \quad 10^4 \le Ra_L \le 10^7 \tag{A.19}$$

$$\overline{Nu_L} = 0.15\sqrt[3]{Ra_L} \quad \text{if} \quad 10^7 < Ra_L \le 10^{11} \tag{A.20}$$

Lower surface of horizontal wall D:

$$\overline{Nu_L} = 0.27\sqrt[4]{Ra_L} \quad \text{if} \quad 10^5 \le Ra_L \le 10^{10} \tag{A.21}$$

Free convection coefficients are weak functions of temperature. Higher temperature differences between wall and surrounding airflow yield higher free convection coefficients. The graphs below show values for the heat transfer coefficient values when wall and flow temperatures differ 0.5 [°C] (figure A.9) and 10 [°C] (figure A.10), with $T_{wall} > T_{flow}$.

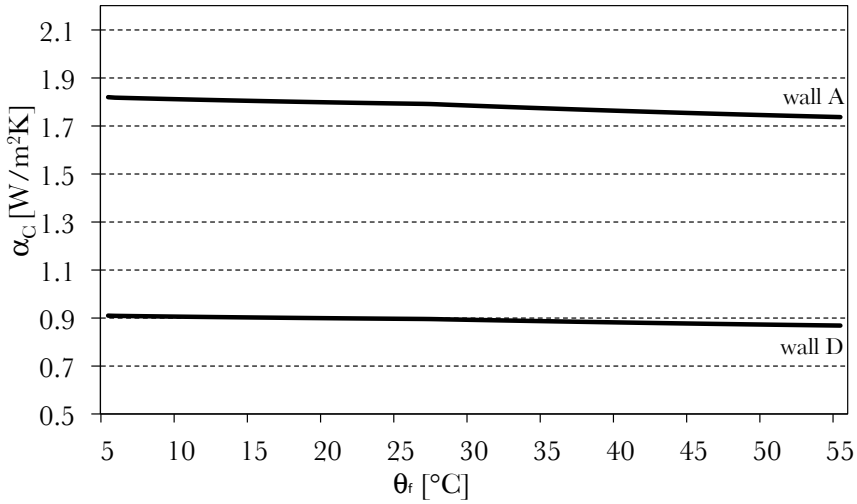

figure A.9 *Free convection heat transfer coefficients as functions of the film temperature between wall and parallel airflow. Free convection coefficients for horizontal wall surfaces A and D are shown for $T_{wall} - T_{flow} = 0.5$ [°C].*

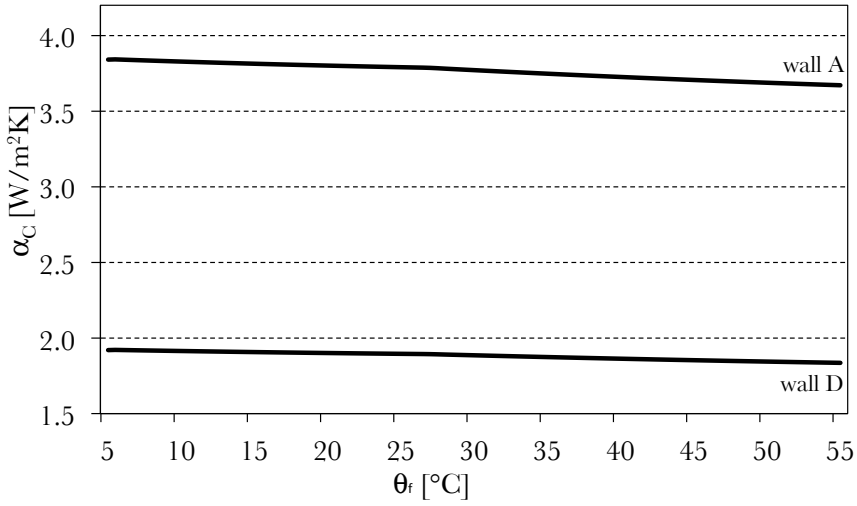

figure A.10 *Free convection heat transfer coefficients as functions of the film temperature between wall and parallel airflow. Free convection coefficients for horizontal wall surfaces A and D are shown for $T_{wall} - T_{flow} = 10$ [°C].*

For free convection along vertical walls in the laminar regime at lower Rayleigh numbers ($Ra<10^5$), Churchill and Chu [7] recommend the following correlation for increased accuracy:

$$\overline{Nu_L} = 0.68 + \frac{0.67\sqrt[4]{Ra_L}}{\left(1 + \left(\frac{0.492}{Pr}\right)^{9/16}\right)^{4/9}} \qquad (A.22)$$

Free convection coefficients are weak functions of temperature. Higher temperature differences between wall and surrounding airflow yield higher free convection coefficients. The graphs below show values for the heat transfer coefficient values for vertical walls in Capacity Cube regions A and D, and B and C, since regions A and D are, like regions B and C, geometrically similar. Wall temperatures and flow temperatures differ 0.5 [°C] (figure A.11) and 10 [°C] (figure A.12), with $T_{wall} > T_{flow}$.

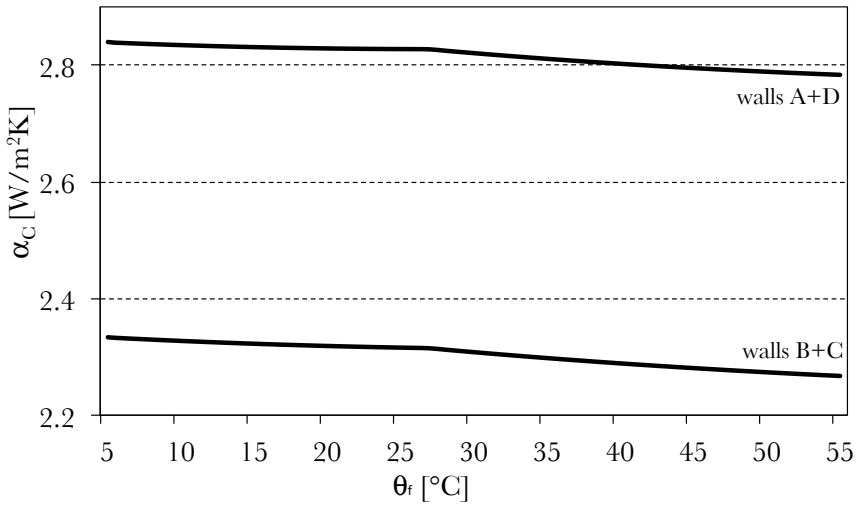

figure A.11 Free convection heat transfer coefficients as functions of the film temperature between vertical walls in CC regions A+D and regions B+C and parallel airflow. Free convection coefficients are shown for $T_{wall} - T_{flow} = 0.5$ [°C].

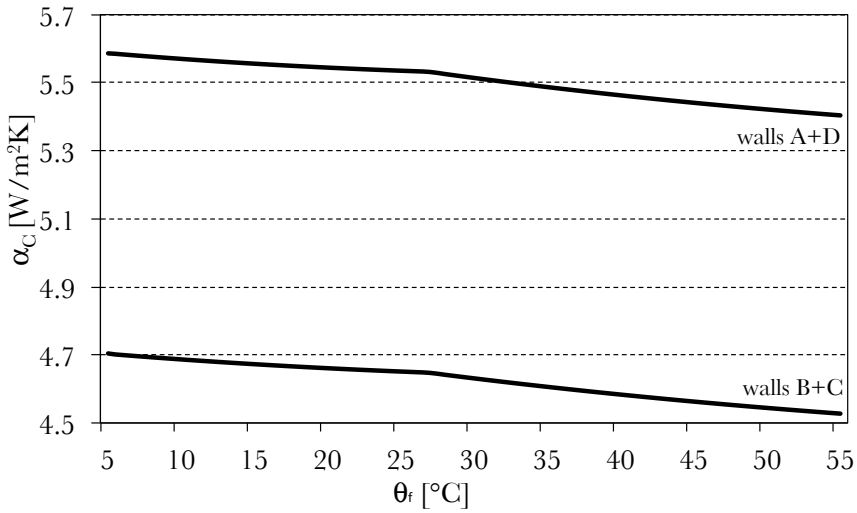

figure A.12 Free convection heat transfer coefficients as functions of the film temperature between vertical walls in CC regions A+D and regions B+C and parallel airflow. Free convection coefficients are shown for $T_{wall} - T_{flow} = 10$ [°C].

In case of combined free and forced convection between horizontal walls and assisting airflow the Nusselt correlation for mixed convection heat transfer is given by [33, p.594]:

$$Nu^3_{mixed} = Nu^3_{forced} + Nu^3_{free} \qquad (A.23)$$

Both free and forced convection coefficients are weak functions of temperature. Accordingly the mixed convection coefficients are weak functions of temperature as well. Regions A and D are geometrically similar. So are regions B and C. The figures below (figure A.13 to figure A.16) show the mixed convection coefficients as functions of air velocity by particular region.

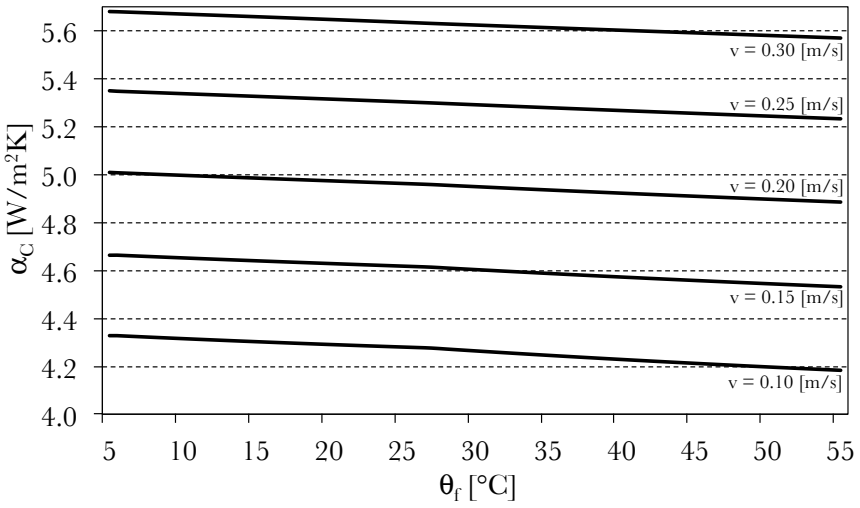

figure A.13 Mixed convection heat transfer coefficients as functions of the film temperature between horizontal wall A and parallel airflow. Mixed convection coefficients for horizontal wall A surface are shown for $T_{wall} - T_{flow} = 10$ [°C].

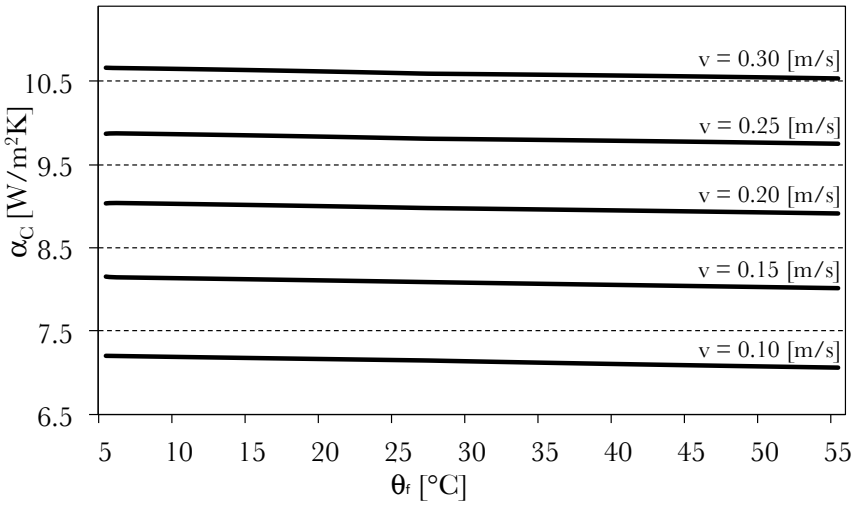

figure A.14 Mixed convection heat transfer coefficients as functions of the film temperature between vertical walls A and D and parallel airflow. Mixed convection coefficients for vertical wall surfaces are shown for $T_{wall} - T_{flow} = 10$ [°C].

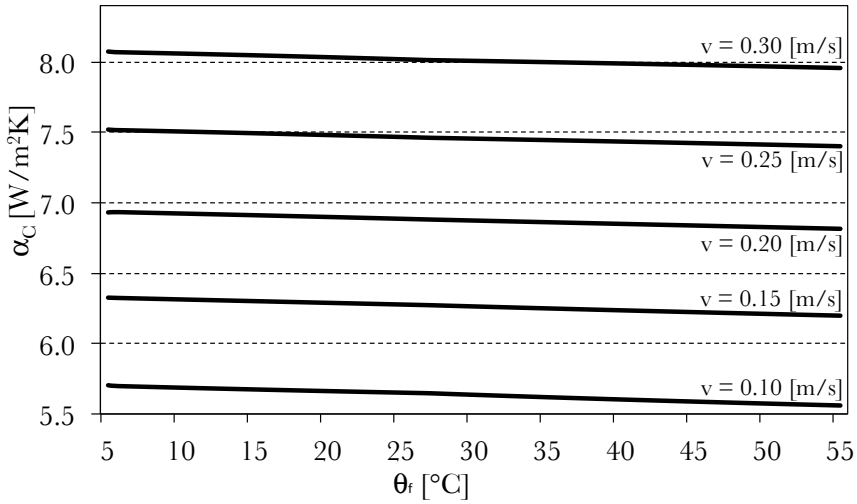

figure A.15 Mixed convection heat transfer coefficients as functions of the film temperature between vertical walls B and C and parallel airflow. Mixed convection coefficients for vertical wall surfaces are shown for $T_{wall} - T_{flow} = 10$ [°C].

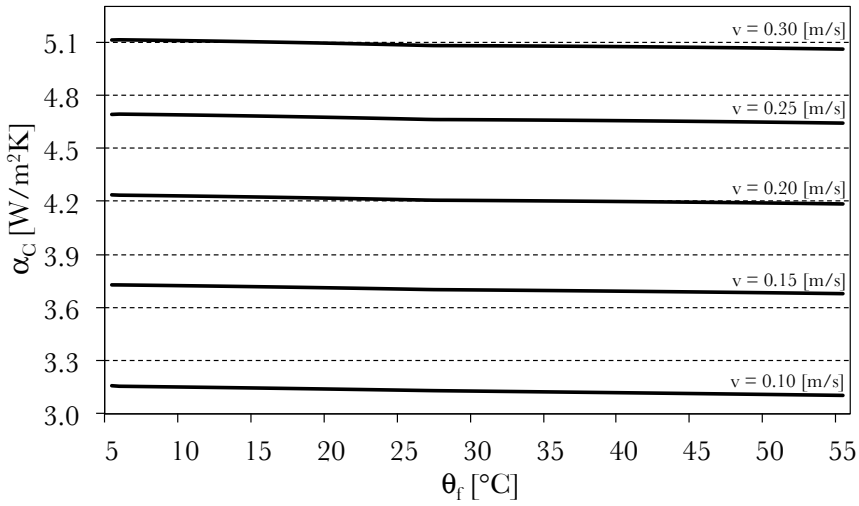

figure A.16 Mixed convection heat transfer coefficients as functions of the film temperature between horizontal wall D and parallel airflow. Mixed convection coefficients for horizontal wall D surface are shown for $T_{wall} - T_{flow} = 10$ [°C].

B.3 Convection: transverse flow through grids

Heat transfer coefficients for perforated plates facing normal to oncoming flows have been investigated by Sparrow and Carranco Ortiz [60]. The recommended Nusselt correlation yields:

$$Nu_D = 0.881 Re^{0.476} \sqrt[3]{Pr} \qquad (A.24)$$

Where the Reynolds number is written in terms of the mass flow that passes the total array of holes:

$$Re = \frac{4f}{N\mu\pi D} \qquad (A.25)$$

The number of holes (N) follows from the open surface area and the hole diameter (D) as given by the manufacturer of the grid (figure A.17). The surface area of a single grid applied in the Capacity Cube is 0.605 [m^2]. Typical hole diameter is 4.8 [mm]. Since the free open surface is 32%, the number of holes in a 0.605 [m^2] grid is approximately 10868.

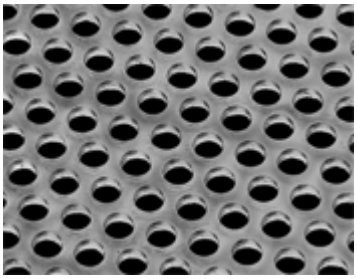

figure A.17 Grid by McNichols [45] (not to scale) as used to guide the airflow within the Capacity Cube. The total surface area is 0.605 [m^2] of which 32% is occupied by 4.8 [mm] diameter holes. Hence, the number of holes in a single grid is approximately 10868.

Heat transfer coefficients between airflow and grids are weak functions of temperature (figure A.18). Higher flow speeds yield higher convection coefficients.

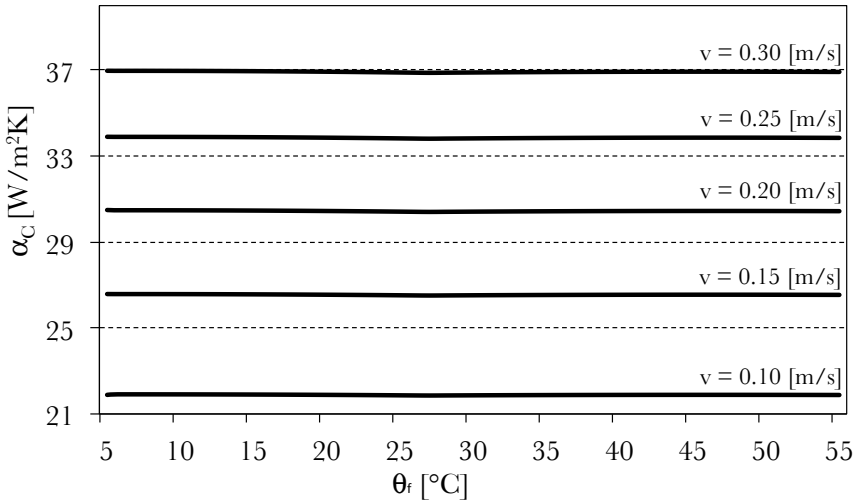

figure A.18 Convective heat transfer coefficients between grids and airflow as a function of air temperature. For air velocities up to 0.3 [m/s] the convection coefficient reaches becomes 37 [W/m²K].

B.4 Convection: external flow along the outer walls

At the outside of the Capacity Cube only free convection effects are present. Although, contrary to the Capacity Cube indoor temperatures, the temperature of the surroundings remains constant, free convection at the outer walls is similar to free convection at the inner walls of the Capacity Cube. For free convection at the outer vertical walls equation (A.22) is valid, whereas for free convection at the outer horizontal walls equations (A.19) to (A.21) are applicable.

Free convection at vertical walls (equation A.22):

$$\overline{Nu_L} = 0.68 + \frac{0.67\sqrt[4]{Ra_L}}{\left(1+\left(\frac{0.492}{Pr}\right)^{9/16}\right)^{4/9}}$$

Free convection along horizontal walls (equations A.19 to A.21):

Upper surface of hot wall ($T_{wall}>T_{surr}$) or lower surface of cold wall ($T_{wall}<T_{surr}$)

$$\overline{Nu_L} = 0.54\sqrt[4]{Ra_L} \quad \text{if} \quad 10^4 \le Ra_L \le 10^7$$

$$\overline{Nu_L} = 0.15\sqrt[3]{Ra_L} \quad \text{if} \quad 10^7 < Ra_L \le 10^{11}$$

Lower surface of hot wall ($T_{wall}>T_{surr}$) or upper surface of cold wall ($T_{wall}<T_{surr}$)

$$\overline{Nu_L} = 0.27\sqrt[4]{Ra_L} \quad \text{if} \quad 10^5 \le Ra_L \le 10^{10}$$

In case the surrounding air temperature surpasses the wall temperature the Grashof number and therefore the Rayleigh number become negative, which implies inverse buoyancy effects. Hence, if the wall temperature successively takes on values below and above the surrounding air temperature, the free convection coefficients as a function of temperature are zero for $T_{wall} = T_{surr}$ and the graph is symmetrical with respect to the surrounding air temperature (figure A.19).

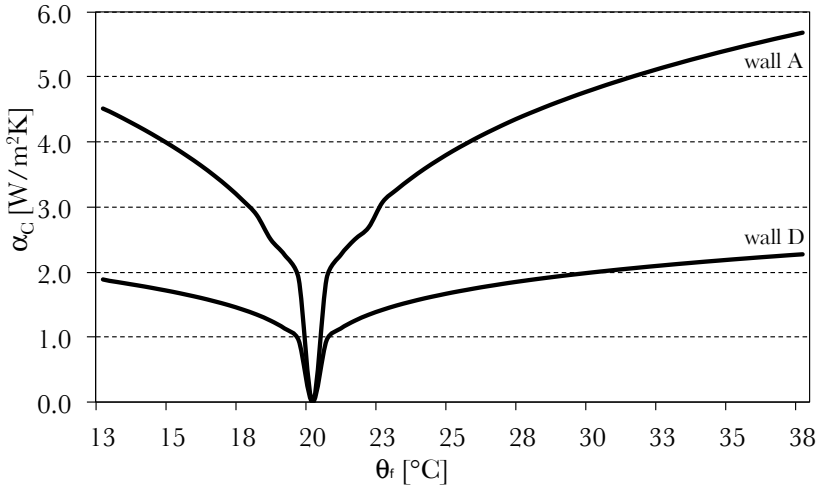

figure A.19 *Free convection heat transfer coefficients as functions of the film temperature between surrounding air and outer horizontal walls in CC regions A and D. The surrounding air temperature is assumed constant at 20 [°C].*

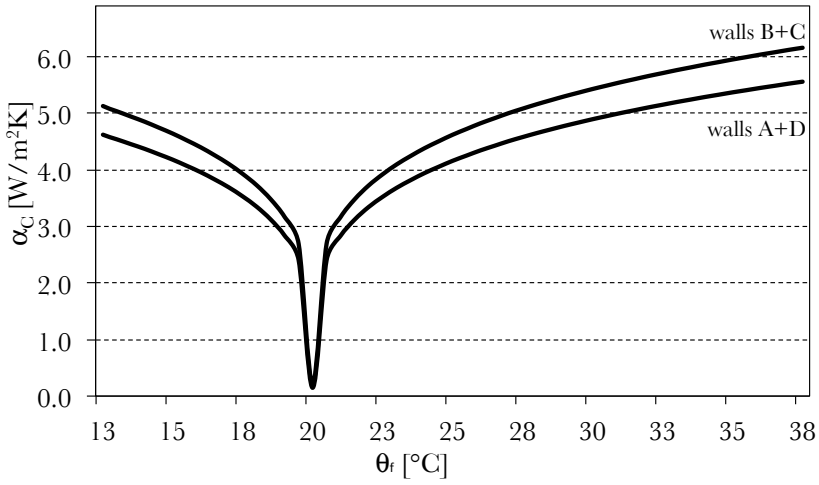

figure A.20 *Free convection heat transfer coefficients as functions of the film temperature between surrounding air and outer vertical walls in CC regions A+D and regions B+C. The surrounding air temperature is assumed constant at 20 [°C].*

Appendix C Heat radiation coefficients

The fundamental equation of heat transfer by radiation between two surfaces m and n is given by:

$$Q_R = \sigma \varepsilon_m F_{m-n} A_m \left(T_m^4 - T_n^4 \right) \tag{A.26}$$

Under certain conditions, analogous to the heat transfer equations of conduction and convection, equation (A.26) may be written as $Q = \alpha A \Delta T$, where α characterizes the overall heat transfer coefficient for radiative heat transmission. Introducing such a radiative heat transfer coefficient the heat radiation from surface m to n is approximated by:

$$Q_R = \alpha_R A_m \left(T_m - T_n \right) \tag{A.27}$$

Where the radiative heat transfer coefficient equals:

$$\alpha_R = \sigma \varepsilon_m F_{m-n} \frac{T_m^4 - T_n^4}{T_m - T_n} \tag{A.28}$$

Expanding the quotient of temperature terms yields:

$$\alpha_R = \sigma \varepsilon_m F_{m-n} \left(T_m^3 + T_m T_n^2 + T_m^2 T_n + T_n^3 \right) \tag{A.29}$$

Since the temperature differences between mutual walls or between PCM pouch and surrounding walls are relatively small over the applied temperature range ($T_m/T_n \approx 1$), the radiative heat transfer coefficient can be expressed as a function of mean surface temperature:

$$\alpha_R = 4 \sigma \varepsilon_m F_{m-n} \overline{T}_{m-n}^3 \tag{A.30}$$

It turns out that radiative heat transfer coefficients are weak functions of the averaged surface temperature for selected view factors and emissivity values (figure A.21 and figure A.22), particularly in the lower temperature range and specifically for low view factor values. Internal polystyrene walls emissivity values are assumed constant at $\varepsilon = 0.73$ [14]. PCM pouches are packed in aluminium foil which emissivity values range from 0.03 to 0.94 [6, 34]. Accounting for some fouling at the pouch surface, the PCM pouch emissivity value is assumed constant at $\varepsilon = 0.8$.

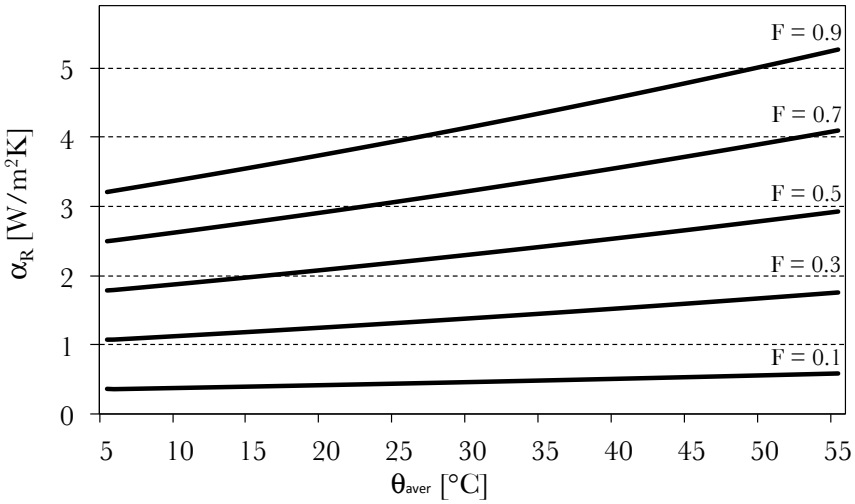

figure A.21 Radiative heat transfer coefficients as functions of the averaged surface temperature. Heat transfer coefficients are shown at selected view factors (F) for Capacity Cube polystyrene inner walls with an emissivity of 0.73.

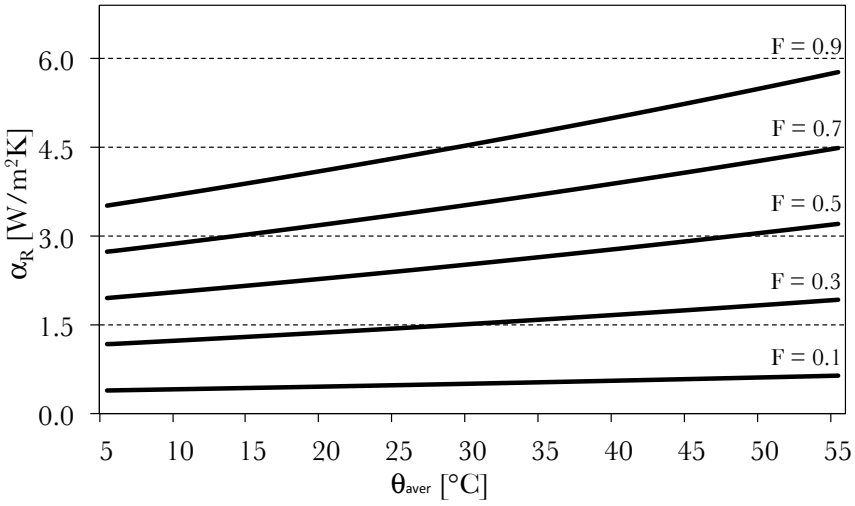

figure A.22 Radiative heat transfer coefficients as functions of the averaged surface temperature. Heat transfer coefficients are shown at selected view factors (F) for aluminium covered PCM pouches with an emissivity of 0.8.

View factor $F_{n\text{-}m}$ is defined as the portion of radiation that leaves surface n and reaches surface m. Theoretically view factors equal zero if surfaces do not 'see' each other at all, and view factors equal unity when a surface is fully surrounded by another surface. In practice view factors will have values in between zero and unity (

table A.2). View factors are calculated according to the geometries described by Howell [31]:

Parallel rectangles:

$$F_{m-n} = \frac{2d^2}{\pi LW}\left\{\ln\left[\frac{\left(1+\frac{L^2}{d^2}\right)\left(1+\frac{W^2}{d^2}\right)}{1+\frac{L^2}{d^2}+\frac{W^2}{d^2}}\right]^{1/2} + \ldots \right.$$

$$\ldots \frac{L}{d}\sqrt{1+\frac{W^2}{d^2}}\arctan\frac{L}{d\sqrt{1+\frac{W^2}{d^2}}} + \ldots \qquad \text{(A.31)}$$

$$\left. \ldots \frac{W}{d}\sqrt{1+\frac{L^2}{d^2}}\arctan\frac{W}{d\sqrt{1+\frac{L^2}{d^2}}} - \frac{L}{d}\arctan\frac{L}{d} - \frac{W}{d}\arctan\frac{W}{d}\right\}$$

Perpendicular rectangles:

$$F_{m-n} = \frac{W}{\pi L}\left\{\frac{L}{W}\arctan\frac{W}{L} + \frac{H}{W}\arctan\frac{W}{H} - \ldots \right.$$

$$\ldots \sqrt{\left(\frac{H^2}{W^2}+\frac{L^2}{W^2}\right)}\arctan\frac{1}{\sqrt{\left(\frac{H^2}{W^2}+\frac{L^2}{W^2}\right)}} + \ldots$$

$$\ldots \frac{1}{4}\ln\left[\frac{\left(1+\frac{L^2}{W^2}\right)\left(1+\frac{H^2}{W^2}\right)}{1+\frac{L^2}{W^2}+\frac{H^2}{W^2}}\left(\frac{\frac{L^2}{W^2}\left(1+\frac{L^2}{W^2}+\frac{H^2}{W^2}\right)}{\left(1+\frac{L^2}{W^2}\right)\left(\frac{L^2}{W^2}+\frac{H^2}{W^2}\right)}\right)^{L^2/W^2} \ldots \right. \qquad \text{(A.32)}$$

$$\left. \ldots \left(\frac{\frac{H^2}{W^2}\left(1+\frac{H^2}{W^2}+\frac{L^2}{W^2}\right)}{\left(1+\frac{H^2}{W^2}\right)\left(\frac{H^2}{W^2}+\frac{L^2}{W^2}\right)}\right)^{H^2/W^2}\right]\right)$$

table A.2 *View factors for all nodes which represent surfaces that mutually transfer heat by radiation. The nodes that represent surfaces facing the environment are left out, since these nodes are fully surrounded, thus their view factors equal unity.*

node m	surface m	A_m [m^2]	node n	surface n	A_n [m^2]	F_{m-n}	F_{n-m}
2	inner horizontal wall A	0.61	5	inner vertical wall A	0.28	0.2	0.4
			8	grid A-B	0.61	0.8	0.8
5	inner vertical wall A	0.28	8	grid A-B	0.61	0.4	0.2
8	grid A-B	0.61	10	inner vertical wall B	0.55	0.3	0.4
			13	'adiabatic' wall B	0.11	0.1	0.3
			14	PCM pouch	0.45	0.6	0.8
10	inner vertical wall B	0.55	13	'adiabatic' wall B	0.11	0.2	0.8
			14	PCM pouch	0.45	0.3	0.3
13	'adiabatic' wall B	0.11	14	PCM pouch	0.45	0.2	0.1
14	PCM pouch	0.45	16	inner vertical wall C	0.55	0.3	0.3
			19	'adiabatic' wall C	0.11	0.1	0.2
			20	grid B-C	0.61	0.8	0.6
16	inner vertical wall C	0.55	19	'adiabatic' wall C	0.11	0.2	0.8
			20	grid B-C	0.61	0.4	0.3
19	'adiabatic' wall C	0.11	20	grid B-C	0.61	0.3	0.1
20	grid B-C	0.61	22	inner vertical wall D	0.28	0.2	0.4
			25	inner horizontal wall D	0.61	0.8	0.8
22	inner vertical wall D	0.28	25	inner horizontal wall D	0.61	0.4	0.2